Supplementary Material

Chromosome engineering:

Our chromosome engineering strategy is based on the Cre/loxP site-specific recombinase system [reviewed in [1]] to generate chromosomal rearrangements [2, 3]. Because the Cre/loxP system is relatively inefficient at mediating inter-chromosomal events (<1 x 10^{-3}), we are using reconstitution of a selectable marker to isolate the cells that undergo Cre-mediated recombination. A schematic representation of this strategy is shown in Supplementary Figure 1. This strategy involves reconstitution of a cloned murine Aprt gene in a human cell line, HTD114, which is APRT deficient [4]. The strategy involves the generation of parental cell clones (P-clones); each containing two independently inserted loxP cassettes. One cassette contains the 5' portion of the Aprt gene linked to a G418 resistance gene (5'AP-loxP), and the other cassette contains the 3' portion of the Aprt gene linked to a Hygromycin B resistance gene (loxP-3'RT). Each cassette contains loxP sites in the second intron of the Aprt gene. Thus, following Cre-mediated recombination, the Aprt gene is reconstituted at the loxP sites within the second intron, and reciprocal exchanges are generated as recombinant clones or pools (R-clones/pools). In addition, work from Dr. M. Jasin's lab indicates that chromosome translocations can be generated from DNA double strand breaks induced by the rare cutting restriction enzyme I-Sce1 [5]. Therefore, as an alternative approach to generate translocations using these same

cassettes, we introduced I-Sce1 recognition sequences into the second intron of the Aprt gene in the 5' and 3' cassettes (Sup. Fig. 1).

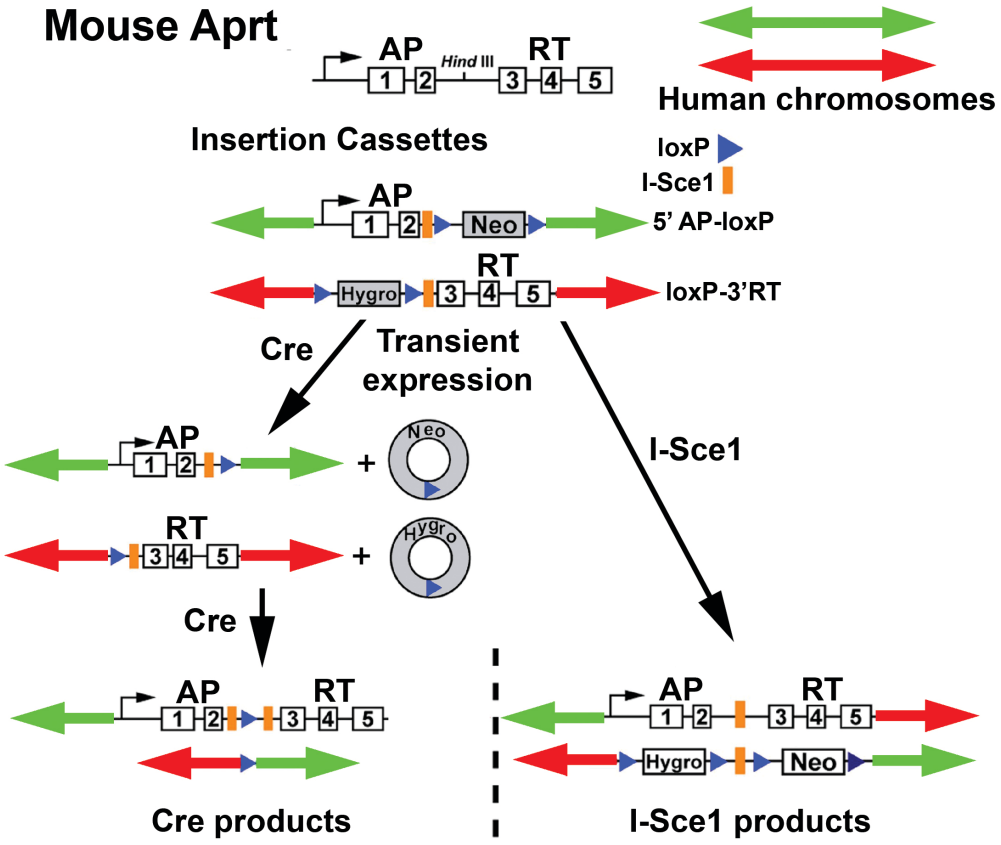

Sup. Fig. 1. Schematic diagram of our chromosome engineering strategy. A diagram of the mouse genomic Aprt gene, with a unique Hind III site in intron 2, is shown. The 5' portion of the Aprt gene was separated from the 3' portion at this unique Hind III site. Floxed Neo or Hyg resistance genes were inserted at the Hind III site in either the 5' or 3' portions of the Aprt gene, respectively, resulting in the 5'AP-loxP and loxP-3'RT cassettes. The 5'AP-loxP and loxP-3'RT cassettes integrate randomly throughout the genome following linearization and electroporation. After Cre transient transfection, reciprocal translocations are generated in a two-step process. First, due to the close proximity of the loxP sites flanking the Neo and Hyg genes, and the fact that they are aligned in the same orientation, the Neo and Hyg genes are excised as circles via highly efficient (determined to be >90%; data not shown) intra-chromosomal events. Next, Cre directs the remaining loxP sites to proceed through a low efficiency (<1 X 10^{-3}) inter-chromosomal reciprocal exchange. This results in reconstitution of the Aprt gene on one derivative chromosome, and a single loxP site on the other derivative, converting cells from $APRT^-$ (P-clones) to $APRT^+$ (R-clones or pools) [2, 3].

This system allows for the generation of chromosome rearrangements at similar breakpoints using two distinct mechanisms: 1) site-specific recombination mediated by Cre, and 2) non-homologous end joining of DNA double strand breaks generated by I-Sce1. One of the advantages of this system is that the same rearrangements can be generated in multiple, independent events. In addition, because the 5' and 3' Aprt cassettes contain Neo and Hyg genes flanked by *loxP* sites (i.e. floxed; see Sup. Fig. 1), Cre-mediated intra-chromosomal deletions of the Neo and Hyg genes can be accomplished without the generation of translocations- owing to the fact that Cre is more efficient when loxP sites are in close proximity [(6)]. These small internal deletions serve as controls for Cre-mediated events at specific chromosomal locations, and to assay any non-specific affects of Cre forced expression [(2)]. Furthermore, deletion of the Neo and Hyg genes allows us to reuse our original 5'AP-loxP and loxP-3'RT cassettes, as the resulting cells are sensitive to G418 or Hygromycin B, respectively.

Balanced Translocations display DRT/DMC.

To identify chromosome translocations that display the DRT/DMC phenotype we previously isolated 97 parental clones, 'P-clones', that contained independent random insertions of the two *Aprt* cassettes. Subsequently, each P-clone was transiently transfected with a Cre expression vector and subsequently cultured in media that selects for Aprt+ cells. Pools of Aprt+ colonies were expanded and harvested for karyotypic analysis. Mitotic spreads from each recombinant pool, "R-pool", were analyzed for the presence of chromosomes with DMC. One important consideration for detection of the DMC phenotype is to

omit a colcemid pretreatment step prior to the mitotic harvest [7]. Therefore, all karyotypic assays for DMC were carried out in the absence of colcemid. We found that the majority of R-pools displayed a relatively low frequency of DMC, ranging from 0-4%. In contrast, 5 R-pools contained chromosomes with DMC in a greater fraction of mitotic spreads, ranging from 6% to 50%.

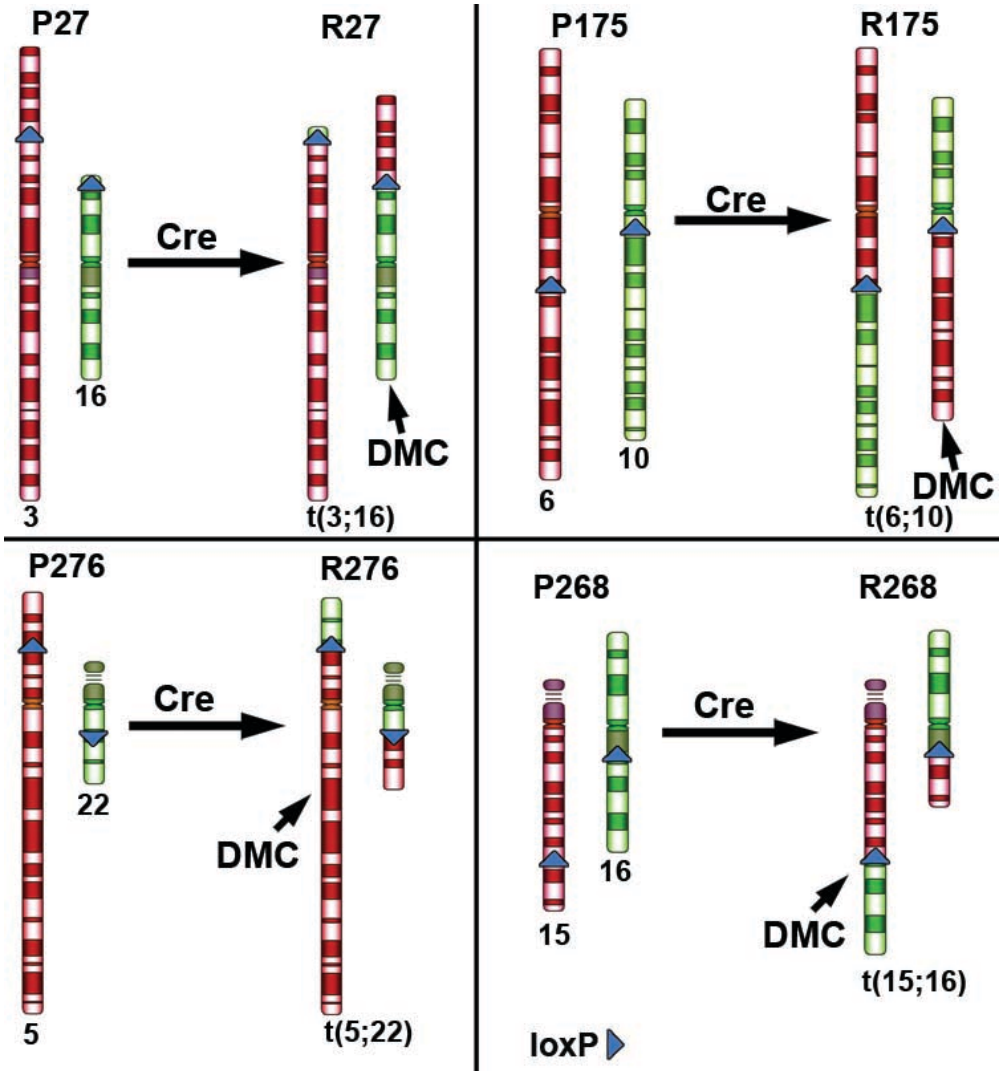

Sup. Fig. 2. DRT/DMC occurs on only one derivative chromosome of certain balanced translocations: A schematic diagram of the t(6;10)(q15;q11.2) in R175, t(15;16)(q24;q12.1) in R268, t(3;16)(p13;p13.3) in R27, t(der5p;22)(p14;q11.2) in R276. Analysis of a fifth balanced translocation, a t(3;13)(q29;q14) present in R186, showed that both derivative chromosomes could display DMC, indicating that the phenotype is not restricted to a single derivative chromosome [2].

This analysis led to the identification of five different balanced translocations that display DRT/DMC [(2); also see Sup. Fig. 2]. In addition, detailed karyotypic analysis of the resulting balanced translocations indicated that, on 4 of 5 translocations, only one derivative chromosome displayed the DMC phenotype (2). For example, Supplementary Figure 3 shows a schematic diagram (panel A), partial G-banded karyotype (panel B), and the DMC phenotype (panel C) on the chromosome 10 derivative of a balanced translocation involving chromosomes 6 and 10. This t(6;10) can be generated by treating the P175 cell line with either Cre or I-Sce1 (see Sup. Fig. 1), selecting for Aprt+ cells, and isolating pools or clones of R175 cells.

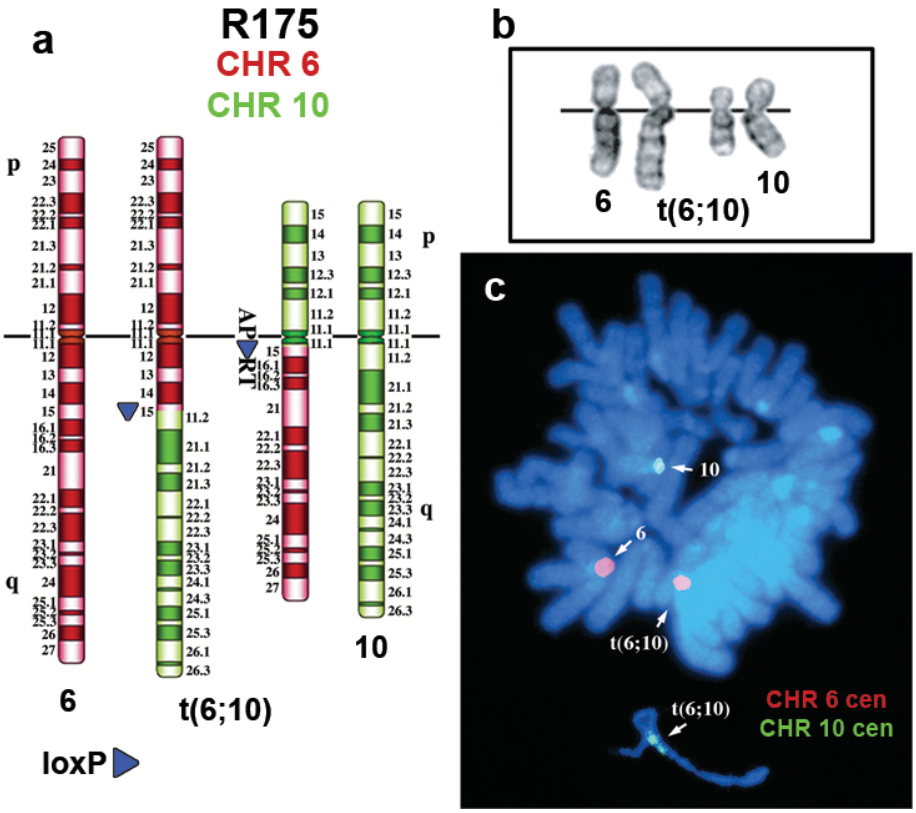

Sup. Fig. 3. DMC on the chromosome 10 derivative of a t(6;10) balanced translocation. A) Schematic diagram, B) G-banded chromosomes, and C) DMC on the chromosome 10 derivative. The approximate location of the reconstituted APRT loxP cassettes are shown (A). Cells were harvested in the absence of colcemid, dropped on slides and processed by FISH using chromosome 6 and 10 centromeric probes (CHR 6 cen and CHR 10 cen). The non-rearranged chromosomes 6 and 10 and the t(6;10) derivatives were identified by reverse DAPI banding (not shown) and are indicated by arrows. P175, and this t(6;10) have been described previously (2).

DRT/DMC and Genomic Instability.

Using this chromosome engineering system we utilized a fluctuation analysis to show that cells containing chromosomes with DRT/DMC have a 30-80 fold increase in the rate at which new gross chromosomal rearrangements occur, indicating that cells with DRT/DMC display translocation instability [(2)]. In addition, we have found that DRT/DMC chromosomes activate the DNA replication and spindle assembly checkpoints [(8)]. Furthermore, cells with DRT/DMC chromosomes have centrosome amplification, abnormal spindle assembly, experience non-disjunction events at an increased frequency, experience endoreduplication and display aneuploid karyotypes, indicating that chromosomes with DRT/DMC are associated with chromosome instability. For these reasons all of the assays carried out in the present study were performed on low passage (<5) cells to ensure that secondary rearrangements and chromosome losses and gains were at a minimum. In addition, because our chromosome engineering system allows for the generation of the same genetic alteration in multiple independent events, all of the replication timing assays for the translocations and deletions, described here, were carried out on multiple independent clones for each genetic alteration.

Alternative Partner analysis.

We previously identified a Cre/loxP-dependent balanced translocation, t(6;10)(q15;q11.2) induced by expressing Cre in the P175 cell line, that displays DRT/DMC [(2), see Sup. Figs. 2 and 3]. To generate 'alternative partner' translocations with both chromosomes 6 and 10, we took advantage of the fact that the loxP cassettes inserted in P175 contain 'floxed' Neo and Hyg genes (see Sup. Fig. 1), and the fact that we had previously generated P175 cells that had deleted both selectable markers via Cre transient expression, but had not generated the t(6;10) [P175ΔNH, (2)]. Deletion of the Neo and Hyg genes allowed us to reuse our original 5'AP-loxP and loxP-3'RT cassettes, as P175ΔNH cells are sensitive to either G418 or Hygromycin B. All of the experiments in this manuscript were carried out with P175ΔNH, and are referred to as simply P175 throughout this report. We isolated 20 clones containing new insertions of the 5'AP-loxP cassette [named P175(5')-1…20] and 20 clones containing the loxP-3'RT cassette [named P175(3')-1…20]. In addition, we have also used Lentiviral vectors, containing new 5'AP and 3'RT loxP cassettes, to integrate new loxP sites into the chromosomes of P175 to generate additional P175(5') and P175(3') clones, see deletion analysis below. We next transiently expressed Cre in each new P175(5') and P175(3') clone and generated Aprt+ clones from each. Note that each new P175(5') and P175(3') clone can potentially generate two different translocations, the original t(6;10) or a new translocation involving either

chromosome 6 or 10 and a new chromosome, depending on the cassette and 'new' integration site (see Fig. 1A).

Chromosome 6 Alternative Partners: We next screened each new Aprt+ clone using Southern blot hybridizations that allowed us to distinguish between the original t(6;10) and any new translocation. Two examples are shown in Sup. Fig. 4. For this analysis we digested genomic DNA, isolated from P175, R175, P175(5')-5, P175(5')-6, and clones R175(5')-5-1…9 and R175(5')-6-1…4, with the BCL-1 restriction enzyme. Note that BCL-1 restriction sites are not present in either of the original loxP cassettes, and therefore the size of the restriction fragment generated by BCL-1 digestion is dependent upon the genomic site of integration. In addition, upon Cre treatment, the size of the BCL-1 restriction fragments are expected to change, with the new size of the fragments dependent on the location of the BCL-1 restriction site present at the genomic integration site of the other partner cassette. For example, BCL-1 digestion of DNA from P175 results in a single relatively large (~20 kb) restriction fragment when probed with the AP half of the Aprt gene (Sup. Fig. 4B and 4C). This ~20 kb band represents the original chromosome 10q11.2 integration site of the 5'AP-loxP cassette. Furthermore, 2 new restriction fragments are generated in R175, ~19kb and ~14kb, suggesting that P175 has two AP cassettes integrated at the same location in chromosome 10. Additional Southern blot analysis of P175 using other restriction enzymes and probes indicated that P175 does indeed contain two

5'AP-loxP cassettes integrated at the same location (not shown). Regardless, the ~19kb and ~14 kb restriction fragments are diagnostic for the t(6;10) present in the original R175 genomic DNA. Supplementary Figure 4 shows the Southern blot hybridizations for two new P175(5') clones, P175(5')-5, and P175(5')-6 and their Aprt positive R175(5')-5 or -6 clones. P175(5')-5 DNA contains a new BCL-1 restriction fragment (~4.5kb) that hybridizes to the AP probe (Sup. Fig. 4B).

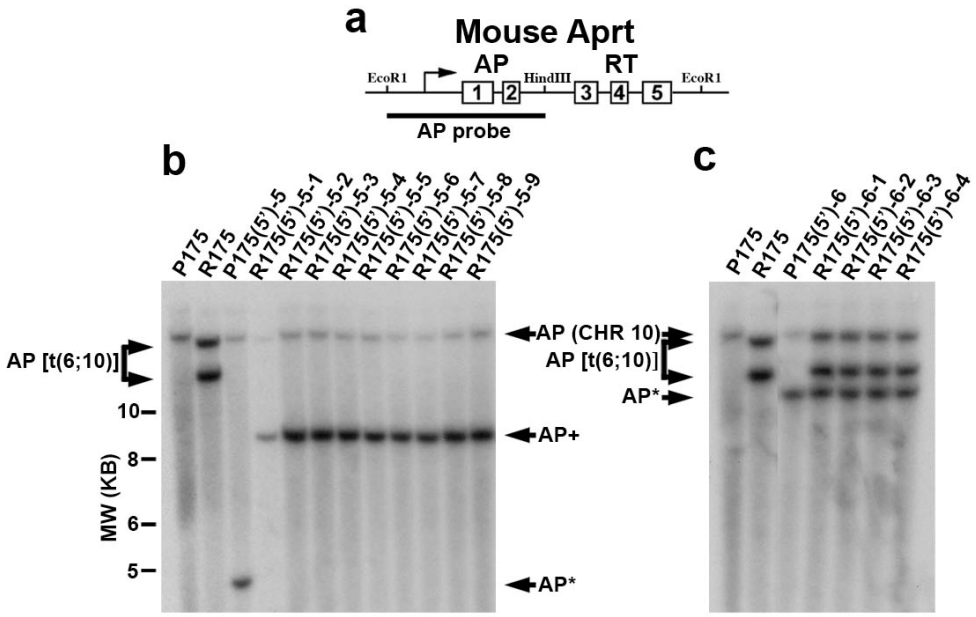

Sup. Fig. 4. Screen for alternative partner translocations. A) Genomic structure of the mouse Aprt gene. B and C) Genomic DNAs from the indicated cell lines were digested with BCL-1, separated on agarose gels, blotted to nylon membranes and probed with the AP probe, as shown in (A). As expected for a single site of integration P175ΔNH contains a single BCL-1 restriction fragment that hybridizes to the AP probe (B and C). In addition, all of the P175(5') clones contain an additional restriction fragment that hybridizes to the AP probe (AP*) but are not present in P175ΔNH (B and C). These new AP restriction fragments represent the 'new' loxP cassette integration sites. The following criteria were used to distinguish between new alternative partner translocations and the original t(6;10) in the R175(5') clones: 1) lack of the ~19kb and ~14kb restriction fragments that are present in the original R175; 2) the presence of a new AP positive restriction fragment in the R175(5') clones (AP+); 3) loss of the AP positive restriction fragment present in the P175(5') clones (AP*); and 4) retention of the original ~20 kb AP restriction fragment [AP(CHR10)]. All of the R175(5')-5 clones pass these criteria (B), and karyotypic analysis of three of the R175(5')-5 clones indicated that they contain a new alternative partner translocation between chromosomes 6 and 17 [t(6;17)(q15;q25); see below]. All of the R175(5')-6 clones fail these criteria (B), and karyotypic analysis of one clone indicated that it contains the original t(6;10), as expected.

This new AP restriction fragment represents the new 5'AP-loxP cassette integrated into another site in the genome. In addition, all of the R175(5')-5 clones have experienced a Cre-mediated event that is distinct from the original R175 rearrangement based on the following criteria: 1) the new AP restriction fragment present in P175(5')-5 is no longer detectable in the R175(5')-5 clones, indicating that the new 5'AP-loxP cassette participated in a Cre-dependent rearrangement; 2) the original ~20kb AP restriction fragment present in P175 is still present in the R175(5')-5 clones, indicating that the original 5'AP-loxP cassette did not experience a Cre-mediated event in these clones; 3) the ~19kb and ~14kb BCL-1 fragments are not present in any of the R175(5')-5 clones, indicating that the t(6;10) was not generated in these clones; and 4) a new BCL-1 restriction fragment (~9kb) is present in the R175(5')-5 clones, indicating that a new Cre-dependent AP fragment was created. All of these changes in restriction fragment size are consistent with a new rearrangement involving chromosome 6 in all of the R175(5')-5 clones. Karyotypic analysis of the R175(5')-5 clones indicated the presence of a new balanced translocation involving chromosomes 6 and 17, t(6;17)(q15;q25) (see Sup. Fig. 5).

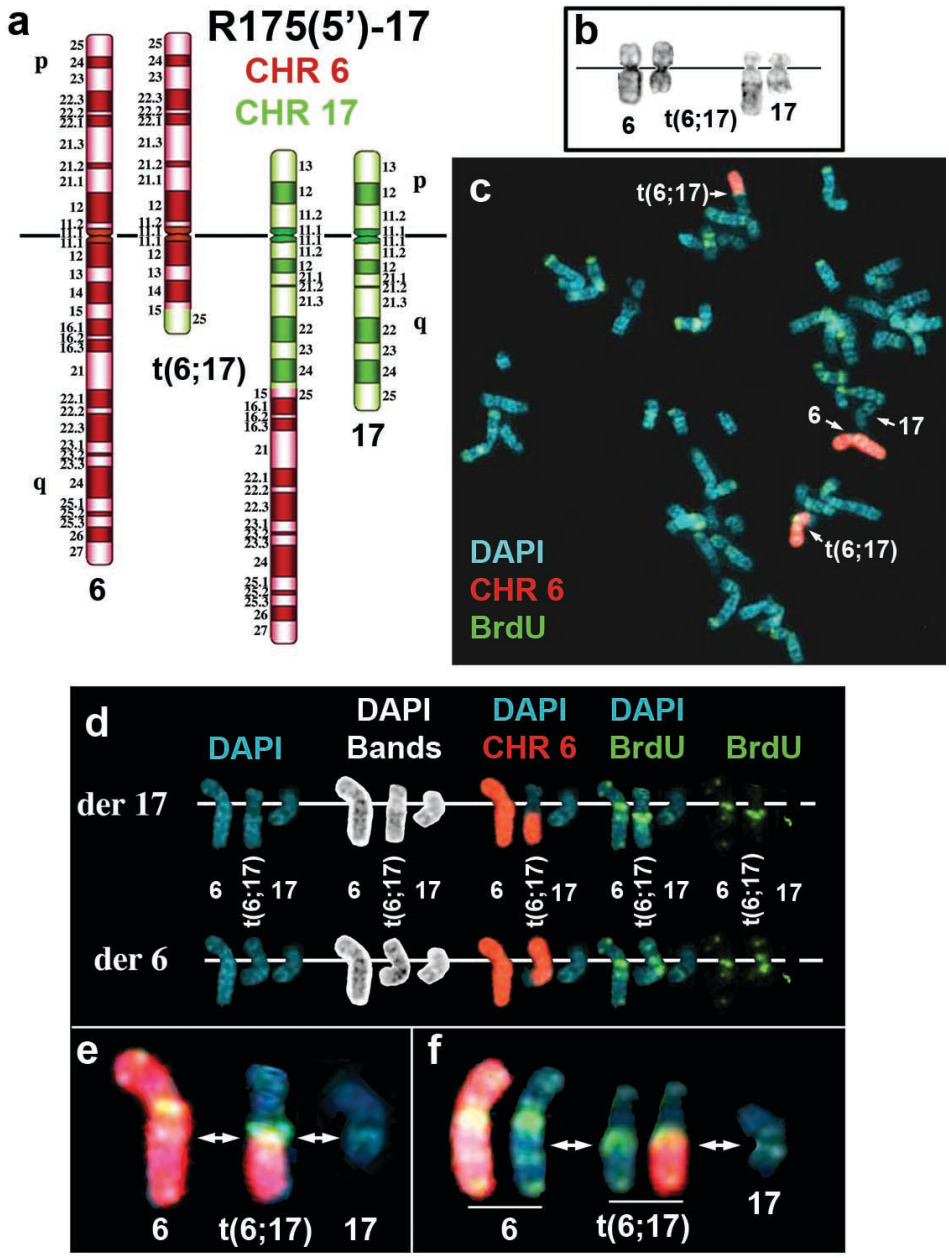

Sup. Fig. 5. Schematic diagram (A), G-banded chromosomes (B), and replication timing assay (C-F) on the t(6;17)(q15;q25). C-E) R175(5')-17 cells were pulsed with BrdU for 4.5 hours, harvested in the absence of colcemid, and processed for FISH using chromosome 6 paint (red) as probe and for BrdU incorporation (green). Inverted DAPI bands were also used to identify the chromosomes (D; DAPI bands). The non-rearranged chromosomes 6 and 17 and the t(6;17) derivatives are indicated by arrows in panel C. C, D, and E represent chromosomes from the same cell. F represents a partial karyotype and BrdU incorporation in a second metaphase cell showing the chromosomes 6, 17 and the chromosome 17 derivative of the t(6;17). Double arrows mark the breakpoints in chromosomes 6 and 17 (E and F). Note the increased BrdU incorporation in the t(6;17).

In contrast, a similar analysis of the Aprt+ R-clones isolated from a different P175(5') clone, P175(5')-6, identified R-clones with the original t(6;10) restriction pattern only (Sup. Fig. 4C). Karyotypic analysis of one of these R175(5')-6 clones indicated the presence of the original t(6;10) (not shown), and were not analyzed further.

Screening additional P175(5') clones, and their respective Aprt+ R175(5') clones using this Southern hybridization scheme, identified three additional 'alternative partner' balanced translocations with chromosome 6 (data not shown): t(6;7)(q15;q36) (Sup. Fig. 6), t(6;9)(q15;p21) (see Fig. 1, and Sup. Figs. 7, and 8), and t(6;8)(q15;q24.1) (Sup. Fig. 9).

One of the advantages of our system is that the same balanced translocations can be generated in multiple independent events, which allows for the analysis of the same translocation in independent clones. For example, we isolated 9 independent clones, R175(5')-5-1…9, containing the new t(6;17) translocation (see Sup. Fig. 4B). Therefore, to rule out any clonal variability in replication timing we characterized a minimum of three independent clones containing each of the new alternative partner translocations for the presence of the alternative partner translocation and for replication timing changes (see below).

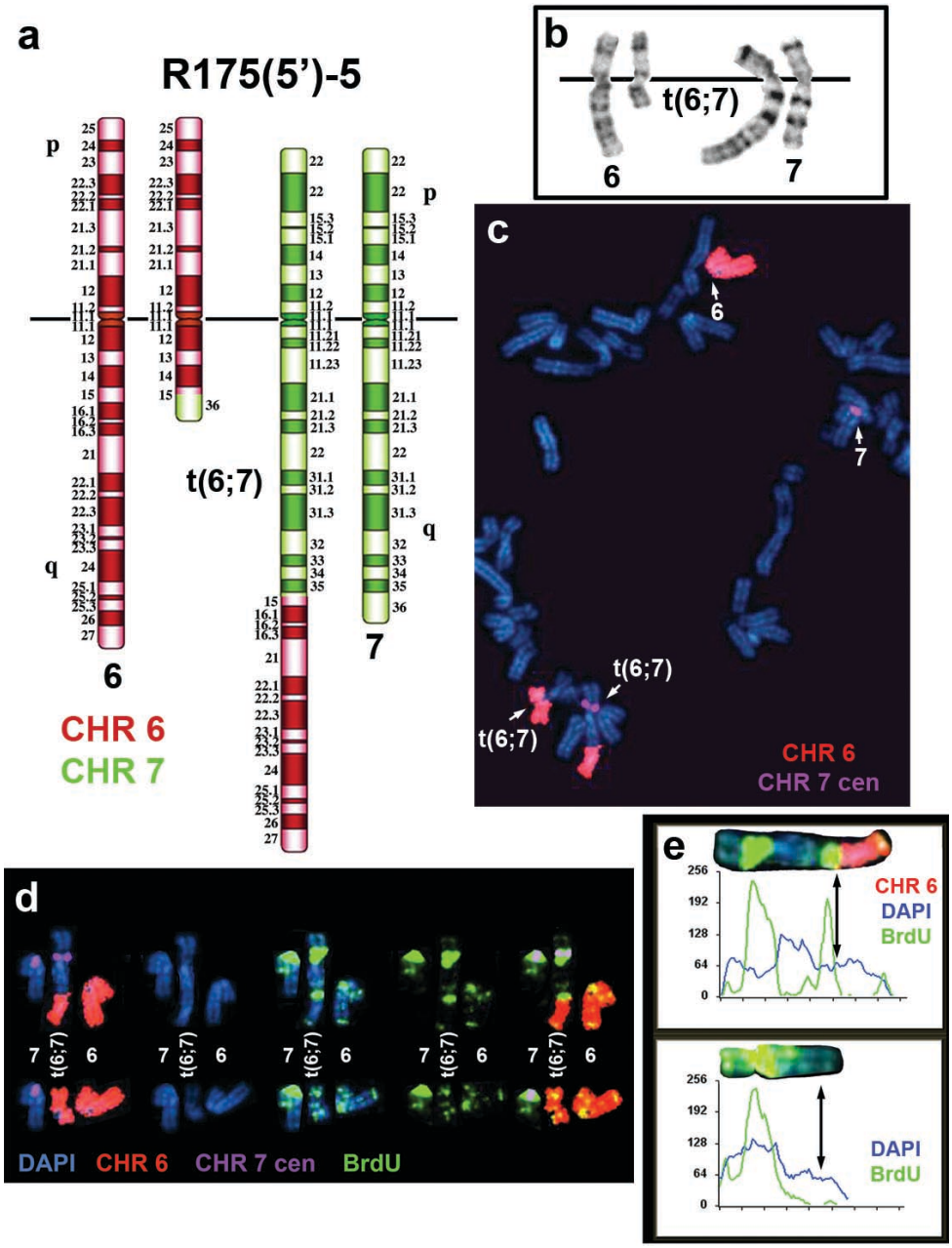

Sup. Fig. 6. Schematic diagram (A), G-banded chromosomes (B), and replication timing assay (C-E) on the t(6;7)(q15;q36). C-E) R175(5')-5 cells were pulsed with BrdU, harvested in the absence of colcemid, and processed for FISH using chromosome 6 paint (red) and chromosome 7 centromeric (purple) probes and for BrdU incorporation (green, not shown in C). Note that the chromosome 7 centromeric probe was pseudo-colored purple for clarity. C, D, and E represent chromosomes from the same cell. The non-rearranged chromosomes 6 and 7 and the t(6;7) derivatives are indicated by arrows (C). E shows the pixel intensity profile for the DAPI staining and BrdU incorporation of the chromosome 7 derivative from the t(6;7) (top panel) and the non-rearranged chromosome 7 (bottom panel). The double arrows indicate the breakpoint.

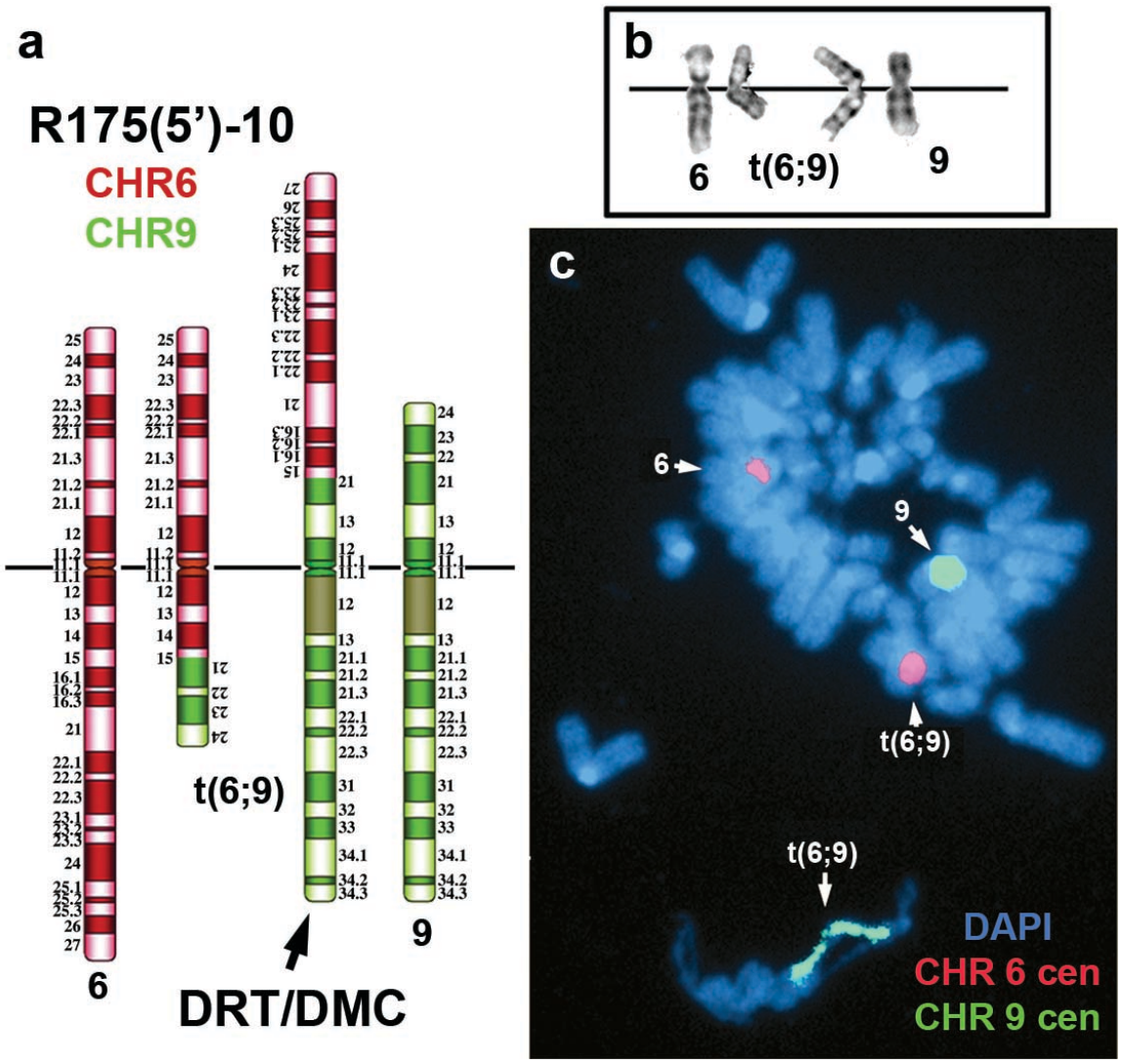

Sup. Fig. 7. Schematic diagram (A), G-banded chromosomes (B), and DMC assay (C) on the t(6;9)(q15;p21). C) R175(5')-10 cells were harvested in the absence of colcemid, and processed for FISH using chromosome 6 paint (red) and chromosome 9 centromeric (green) probes. The non-rearranged chromosomes 6 and 9 and the t(6;9) derivatives are indicated by arrows (C). See Fig. 1 and Sup. Fig. 8 for replication timing assays.

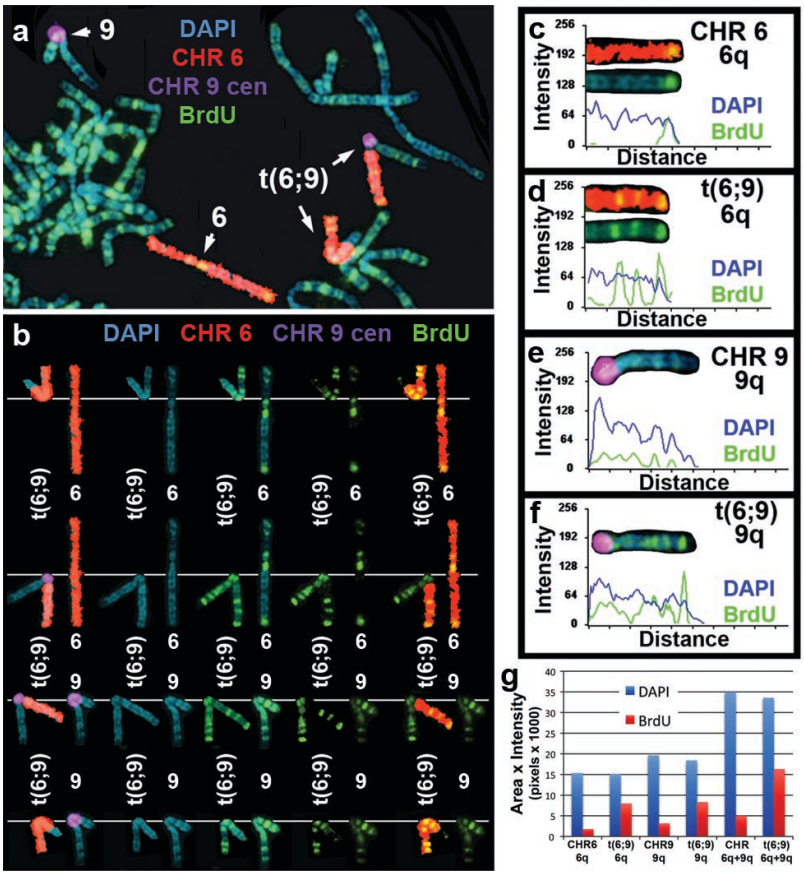

Sup. Fig. 8. Delayed replication on the t(6;9). R175(5')-10 cells were incubated with BrdU for 4.5 hours and processed for BrdU incorporation (green), and for FISH using probes for chromosome 6 (CHR 6 paint, red) and chromosome 9 centromere (CHR 9 cen, purple) (A-F). Note that the chromosome 9 centromeres were pseudo-colored from red to purple for clarity. The arrows mark the non-rearranged chromosomes 6 and 9, and both derivative chromosomes of the t(6;9). B) The non-rearranged chromosomes 6 and 9 were aligned with both derivative chromosomes of the t(6;9). C-F) Pixel intensity profiles of the BrdU incorporation, and DAPI staining along the long arm (q) of the non-rearranged chromosome 6 (C), the long arm of chromosome 6 of the chromosome 9 derivative of the t(6;9) (D), the long arm of the non-rearranged 9 (E), and the chromosome 9 long arm of the t(6;9) (F). The intensity profiles are aligned with the cut out long arms of chromosome 6 (red) or chromosome 9 (purple centromere) for each chromosome (C and D or E and F, resectively). Note that the intensity profile for the BrdU incorporation on 6q of the t(6;9) (D) shows three major peaks (i.e. bands) on the chromosome 6 long arm portion, while the long arm of the non-rearranged chromosome 6 shows only a single peak of incorporation near the telomere (C). Similarly, the intensity profile for the BrdU incorporation in the chromosome 9 long arm of the chromosome 9 derivative (F) shows much more incorporation than the long arm of the non-rearranged chromosome 9 (E). The intensity profiles are aligned with the cut out of the long arms of chromosome 9 for each chromosome (E and F). G) Quantification of the total amount (Area x Intensity) of BrdU incorporation (red) and DAPI staining (blue) on the long arm of the non-rearranged chromosome 6 (CHR6 6q), the long arm of chromosome 6 on the t(6;9) [t(6;9) 6q], the long arm of chromosome 9 (CHR 9q), the long arm of chromosome 9 on the t(6;9) [t(6;9) 9q], the long arm of chromosome 6 plus the long arm of chromosome 9 on the non-rearranged chromosomes (CHR 6q + 9q), and both arms of the t(6;9) [t(6;9) 6q + 9q].

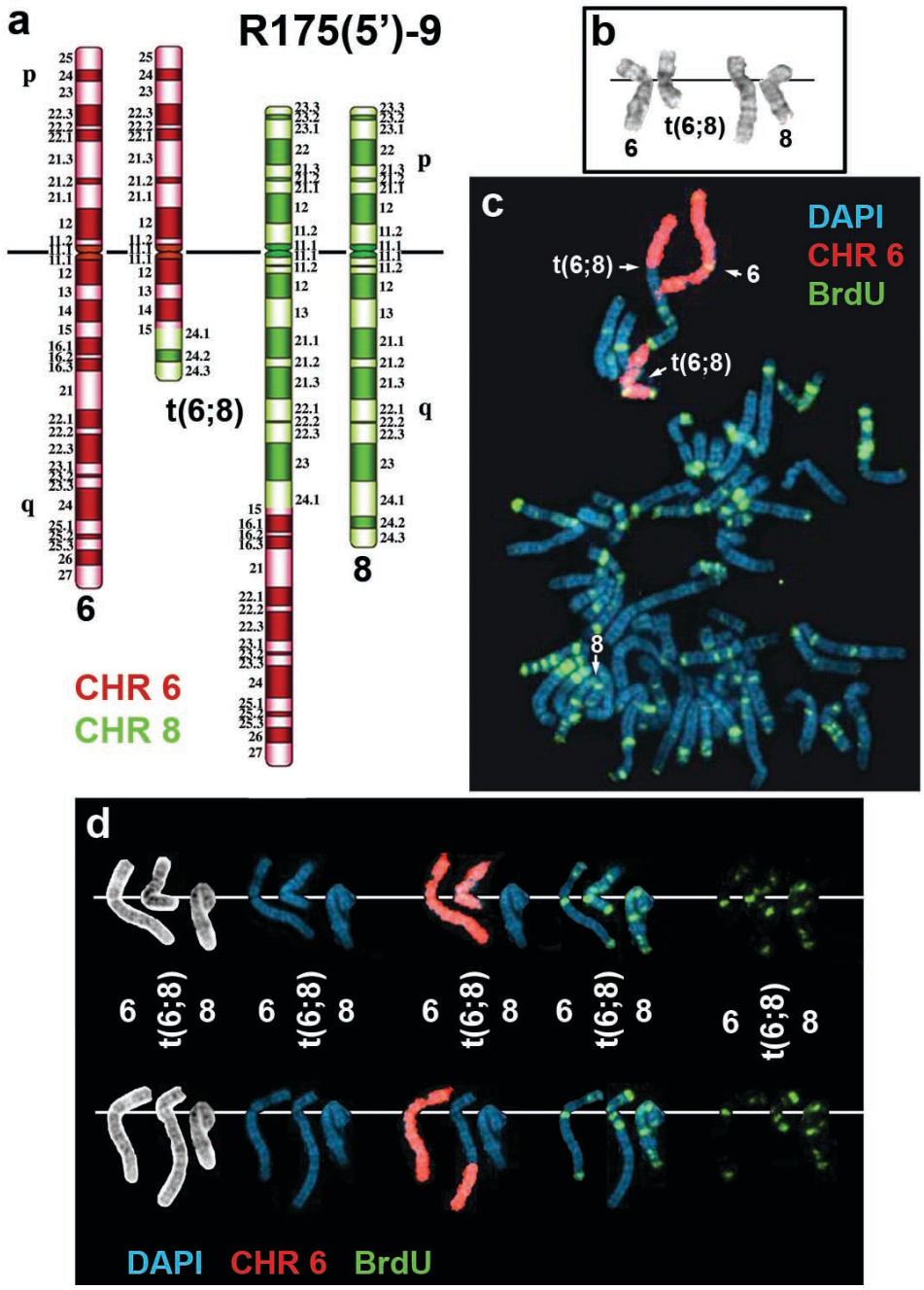

Sup. Fig. 9. Schematic diagram (A), G-banded chromosomes (B), and replication timing assay (C and D) on the t(6;8)(q15;q24.1). C and D) R175(5')-9 cells were pulsed with BrdU, harvested in the absence of colcemid, and processed for FISH using a chromosome 6 paint (red) as probe and for BrdU incorporation (green). Inverted DAPI bands were also used to identify the chromosomes (D, black and white). The non-rearranged chromosomes 6 and 8 and the t(6;8) derivatives are indicated by arrows (C). The BrdU incorporation of the derivative chromosomes 6 (top line) and 8 (bottom line) of the t(6;8) are compared to the non-rearranged chromosomes 6 and 8 (D). C and D represent chromosomes from the same cell.

Chromosome 10 Alternative Partners: Using a similar Southern hybridization screening strategy, as described above for the chromosome 6 alternative partners, we analyzed new P175(3') and Aprt+ R175(3') clones for new rearrangements involving chromosome 10. We processed the BCL-1 digested genomic DNA by Southern blot hybridizations using the 3'RT half of the Aprt gene as probe (data not sown). This allowed us to distinguish between the original t(6;10) and new translocations involving chromosome 10. From this analysis we identified three new balanced translocations involving chromosome 10, a t(1;10)(p23;q11.2), a t(4;10)(q25;q11.2), and a t(5;10)(q35.1;q11.2) (Sup. Figs. 10-12, respectively).

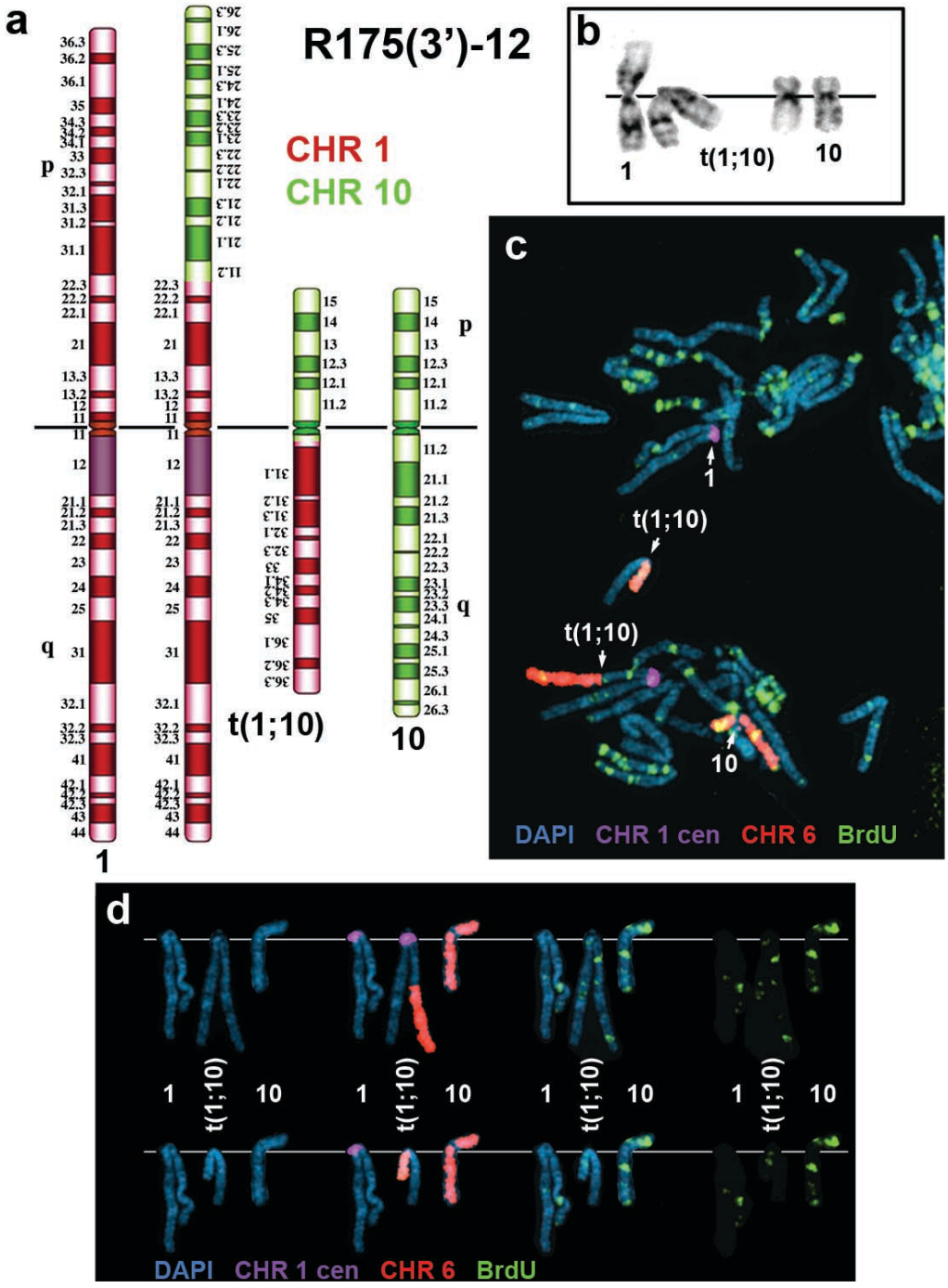

Sup. Fig. 10. Schematic diagram (A), G-banded chromosomes (B), and replication timing assay (C and D) on the t(1;10)(p22.3;q11.2). C and D) R175(3')-12 cells were pulsed with BrdU, harvested in the absence of colcemid, and processed for FISH using chromosome 10 paint (red) and chromosome 1 centromeric (purple) probes and for BrdU incorporation (green). The non-rearranged chromosomes 1 and 10 and the t(1;10) derivatives are indicated by arrows (C). The BrdU incorporation into the derivative chromosomes (1 der and 10 der) of the t(1;10) is compared to the non-rearranged chromosomes 1 and 10 (D). C and D represent chromosomes from the same cell.

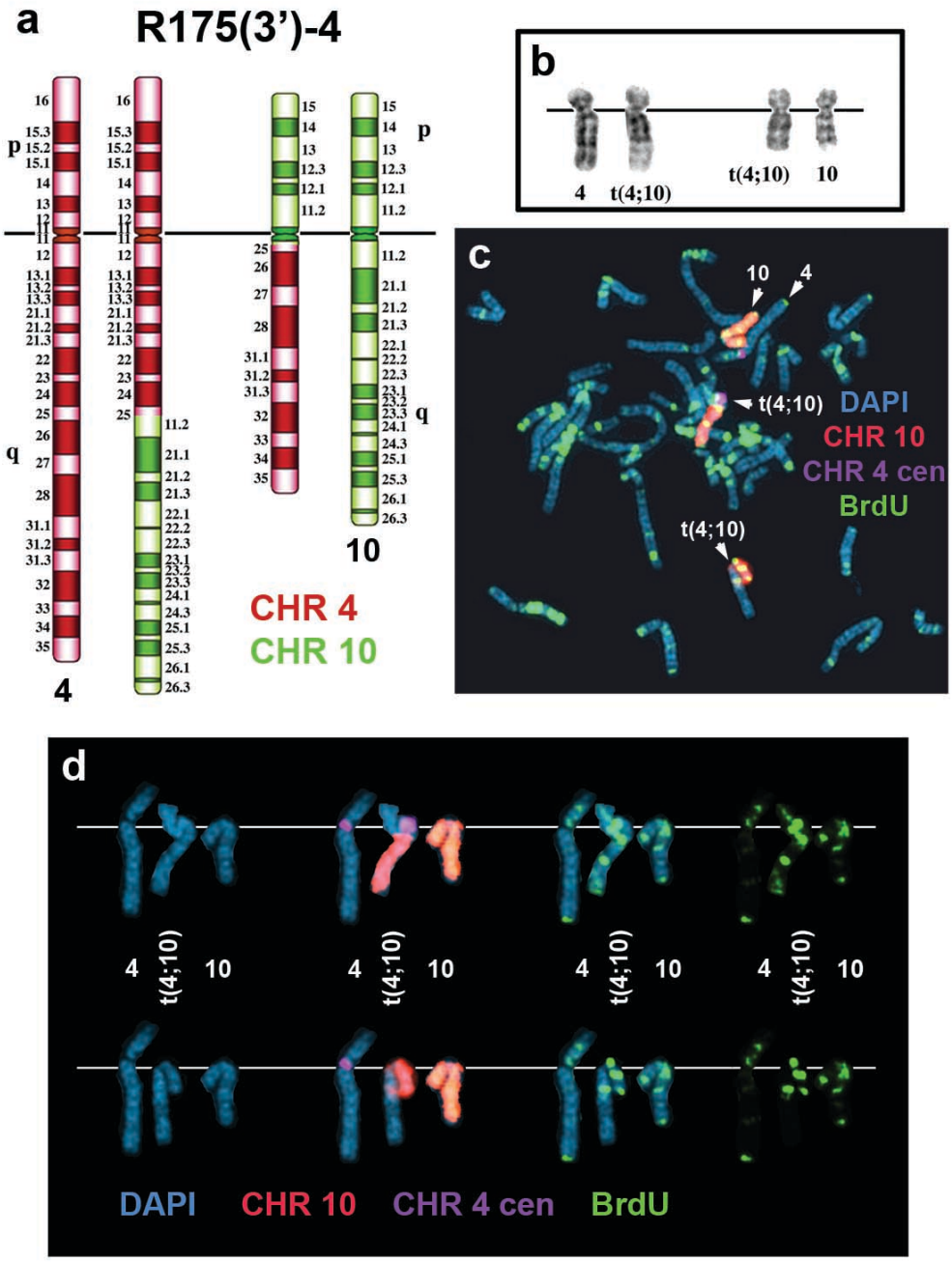

Sup. Fig. 11. Schematic diagram (A), G-banded chromosomes (B), and replication timing assay (C and D) on the t(4;10)(q25;q11.2). C) R175(3')-4 cells were pulsed with BrdU, harvested in the absence of colcemid, and processed for FISH using chromosome 10 paint (red) and chromosome 4 centromeric (purple, pseudo-colored for clarity) probes and for BrdU incorporation (green). The non-rearranged chromosomes 4 and 10 and the t(4;10) derivatives are indicated by arrows (C). The BrdU incorporation into the derivative chromosomes 4 (top line) and 10 (bottom line) of the t(4;10) are compared to the non-rearranged chromosomes 4 and 10 (D). C and D represent chromosomes from the same cell.

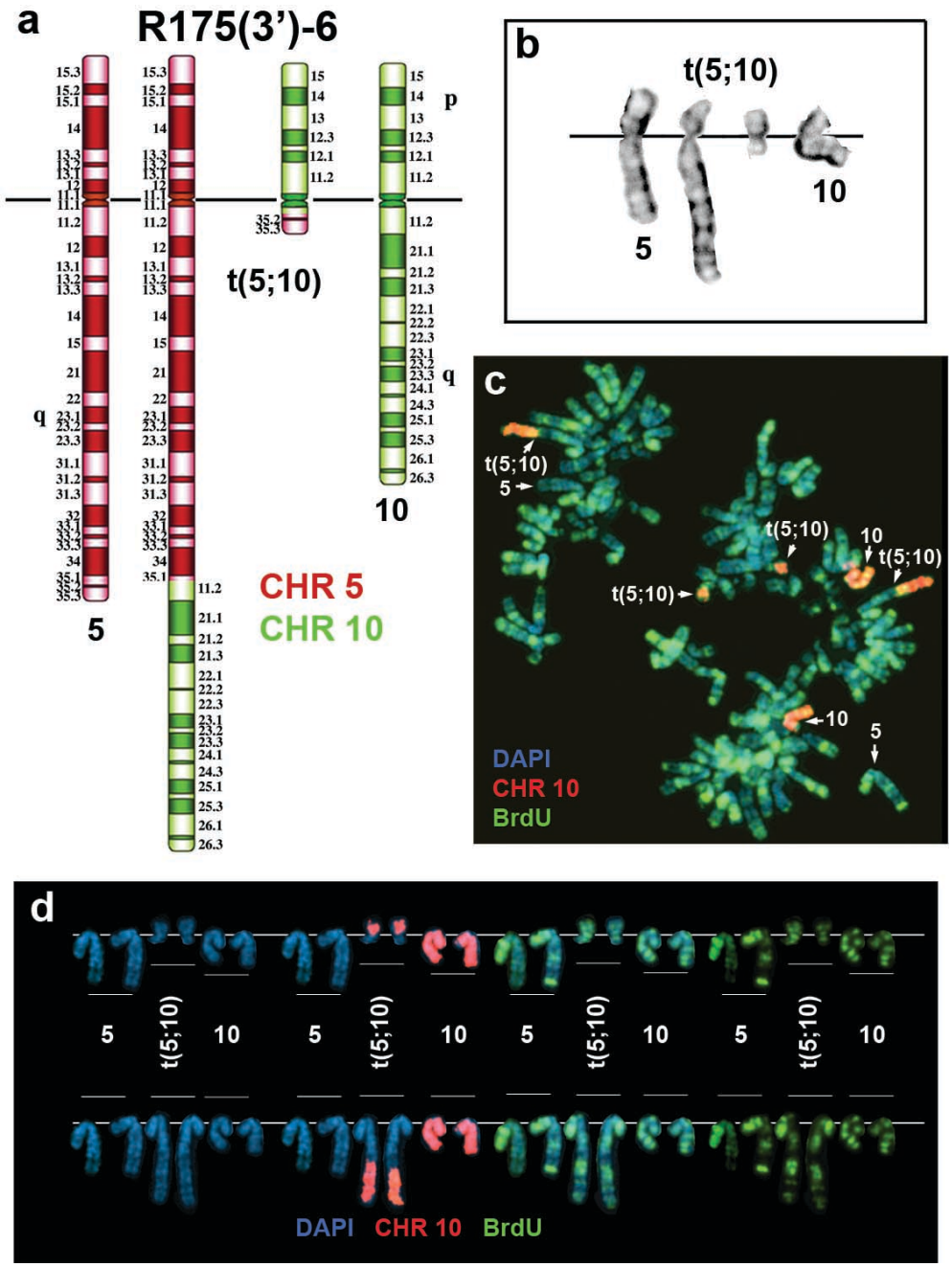

Sup. Fig. 12. Schematic diagram (A), G-banded chromosomes (B), and replication timing assay (C and D) on the t(5;10)(q35.1;q11.2). C and D) R175(3')-6 cells were pulsed with BrdU, harvested in the absence of colcemid, and processed for FISH using a chromosome 10 paint (red) as probe and for BrdU incorporation (green). Inverted DAPI bands were also used to identify the chromosomes from this tetraploid cell (not shown). The non-rearranged chromosomes 5 and 10 and the t(5;10) derivatives are indicated by arrows (C). The BrdU incorporation into the derivative chromosomes 5 (top line) and 10 (bottom line) of the t(5;10) are compared to the non-rearranged chromosomes 5 and 10 (D). C and D represent chromosomes from the same tetraploid cell.

Replication Timing Assay:

The DRT phenotype is characterized by a >2 hour delay in the initiation as well as the completion of DNA synthesis along the entire length of the chromosome, while the other chromosomes within the same cell show normal patterns of DNA synthesis. To characterize the replication timing of the chromosomes involved in this study prior to any Cre-mediated rearrangements we carried out an extensive analysis of chromosome replication timing in parental P175 cells. Our most sensitive assay for detection of DRT was to use pulse labeling with BrdU followed by detection of the incorporated BrdU by fluorescent immunostaining combined with FISH using chromosome-specific probes on metaphase spreads. For this analysis we cultured P175 cells with BrdU for 4.5, 5, 6, 7, 8 and 9 hours and harvested mitotic cells in the absence of a colcemid pretreatment step. This 'terminal labeling' protocol detects the latest replicating regions of chromosomes at the shorter time periods (4.5-6 hours) of BrdU incorporation and middle S-phase plus the late replicating regions during the longer BrdU pulses (7-9 hours; see main text Fig. 1B). Supplementary Figure 13 shows examples of this replication-timing assay for chromosome 6 in P175 cells. The earliest detectable BrdU incorporation, representing the last DNA to replicate, occurred during the 6-hour time point, indicating that G2 in P175 cells was at least 5.5 hours. Note that the two chromosome 6s present in each P175 cell show very similar amounts of BrdU incorporation at each time point and that the 'banded' pattern of

incorporation is similar between the two chromosome 6s within any given cell. In addition, the banded pattern of BrdU incorporation at any given time point is quite similar between cells, and this banded pattern of incorporation is consistent with previous replication timing maps for human chromosome 6 [9, 10]. Furthermore, quantification of the BrdU incorporation was determined for the two chromosome 6s by measuring the total amount of fluorescent signal present. For this analysis we determined the amount of BrdU immunostaining by measuring the pixel intensity along each chromosome, and multiplying the average pixel intensity by the area occupied by those pixels (Sup. Fig. 14A-D). For comparison, we also quantified the total amount of DAPI staining on each chromosome pair using the same metrics (Sup. Fig. 14D). Applying this analysis to 7 different mitotic spreads indicated that the two chromosome 6s within individual P175 cells incorporated very similar amounts BrdU, indicating that the chromosome 6s in P175 replicate synchronously (Sup. Fig. 14E).

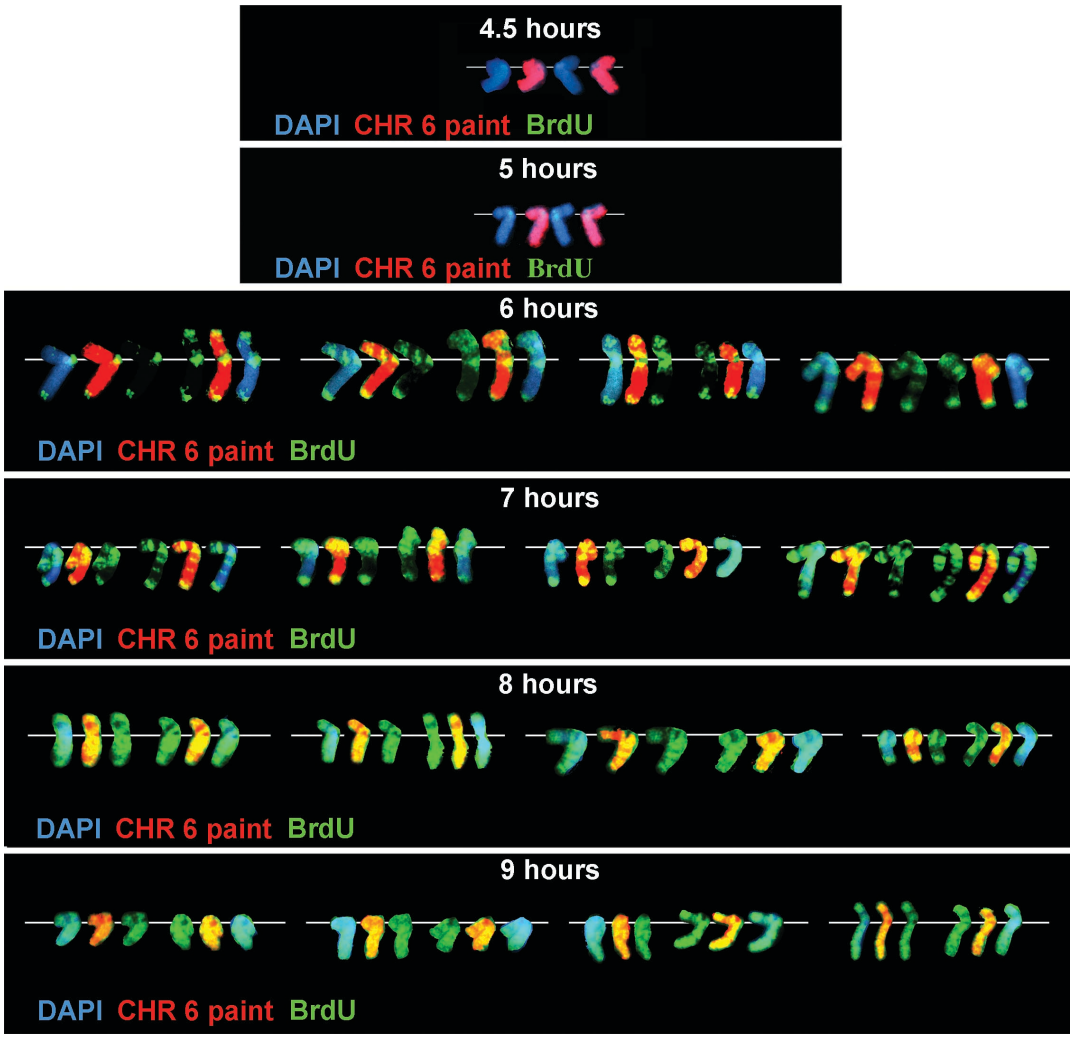

Sup. Fig. 13. Replication timing assay for chromosome 6 in P175. P175 cells were incubated with BrdU for increasing amounts of time followed by mitotic chromosome harvest (see main text Fig. 1B). Fixed cells were dropped on microscope slides and processed for FISH using chromosome-specific paints and for BrdU incorporation. P175 cells were incubated with BrdU for 4.5, 5, 6, 7, 8, and 9 hours, harvested for mitotic chromosomes in the absence of a colcemid pretreatment step, processed for FISH using a chromosome 6 paint (red), stained for BrdU incorporation (green), and counterstained with DAPI (blue). The two chromosome 6s from a single cell, 4.5 and 5 hours, or four different cells, 6, 7, 8, and 9 hours, are aligned with their centromeres positioned on a white line. Note that BrdU incorporation was not detected in any cells in any chromosomes at the 4.5 and 5 hour time points, and only single cells as examples are shown.

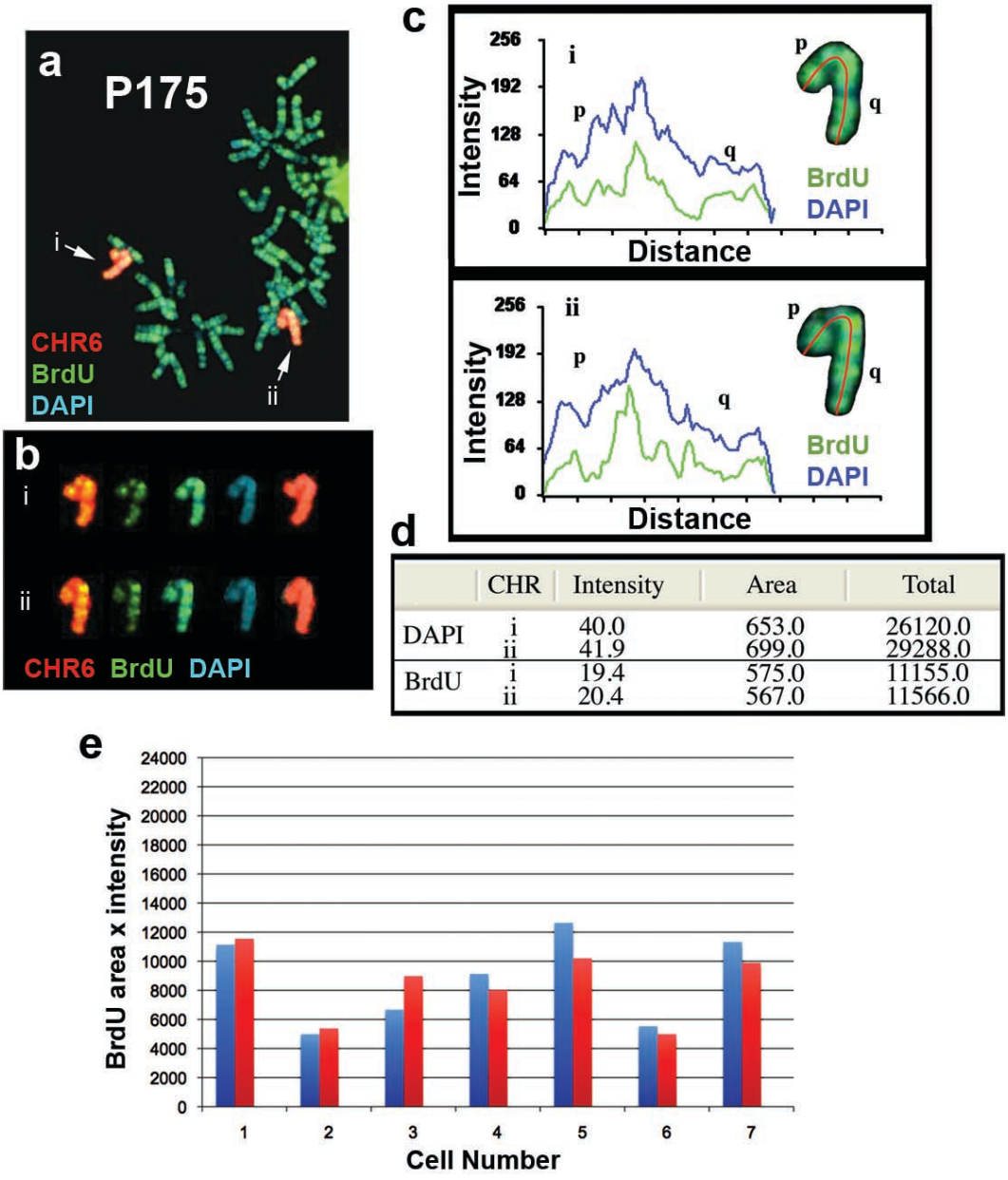

	CHR	Intensity	Area	Total
DAPI	i	40.0	653.0	26120.0
	ii	41.9	699.0	29288.0
BrdU	i	19.4	575.0	11155.0
	ii	20.4	567.0	11566.0

Sup. Fig. 14. Replication timing of chromosome 6 in P175 cells. A) An example of a mitotic spread processed for BrdU incorporation (green) and FISH with a chromosome 6 paint as probe (red). B) The two chromosome 6s were separated from the rest of the spread and the different fluors were overlaid in different combinations. C) Intensity profile of the BrdU incorporation and DAPI staining for the two chromosome 6s shown in panels A and B. The red line on the chromosomes represents the path, starting on the short arm, used to determine the position and location of the signal along the length of each chromosome, the short (p) and long (q) arms are indicated. D) Quantification of the total amount of BrdU incorporation and DAPI staining for the two chromosome 6s shown in panels A-C. The values represent pixels. E) Total BrdU incorporation in the chromosome 6s in P175 cells. The red and blue bars represent the two chromosome 6s from 7 different mitotic cells (Cell Number).

We also carried out a similar replication-timing assay for chromosomes 1, 4, 5, 7, 8, 9, 10, and 17. Supplementary Figure 15 shows this replication-timing assay for chromosome 10 in P175 cells. Note that the two chromosome 10s present in P175 show very similar amounts of BrdU incorporation and that the 'banded' pattern of incorporation is similar between the two chromosomes. The amount of the BrdU incorporation was determined by quantifying the total amount of fluorescent signal present on each chromosome (Sup. Figs. 15C and 15D).

This analysis indicated that the two chromosome 10s in individual P175 cells incorporated very similar amounts of BrdU, indicating that the chromosome 10s replicate synchronously in P175 cells (Sup. Fig. 15E). A similar replication timing analysis indicated that the replication timing of chromosomes 1, 4, 5, 7, 8, 9, and 17 was synchronous between homologous pairs (Sup. Fig. 16), and that the banded pattern of BrdU incorporation (not shown) was consistent with the known replication timing maps for each of these chromosome pairs [9, 10].

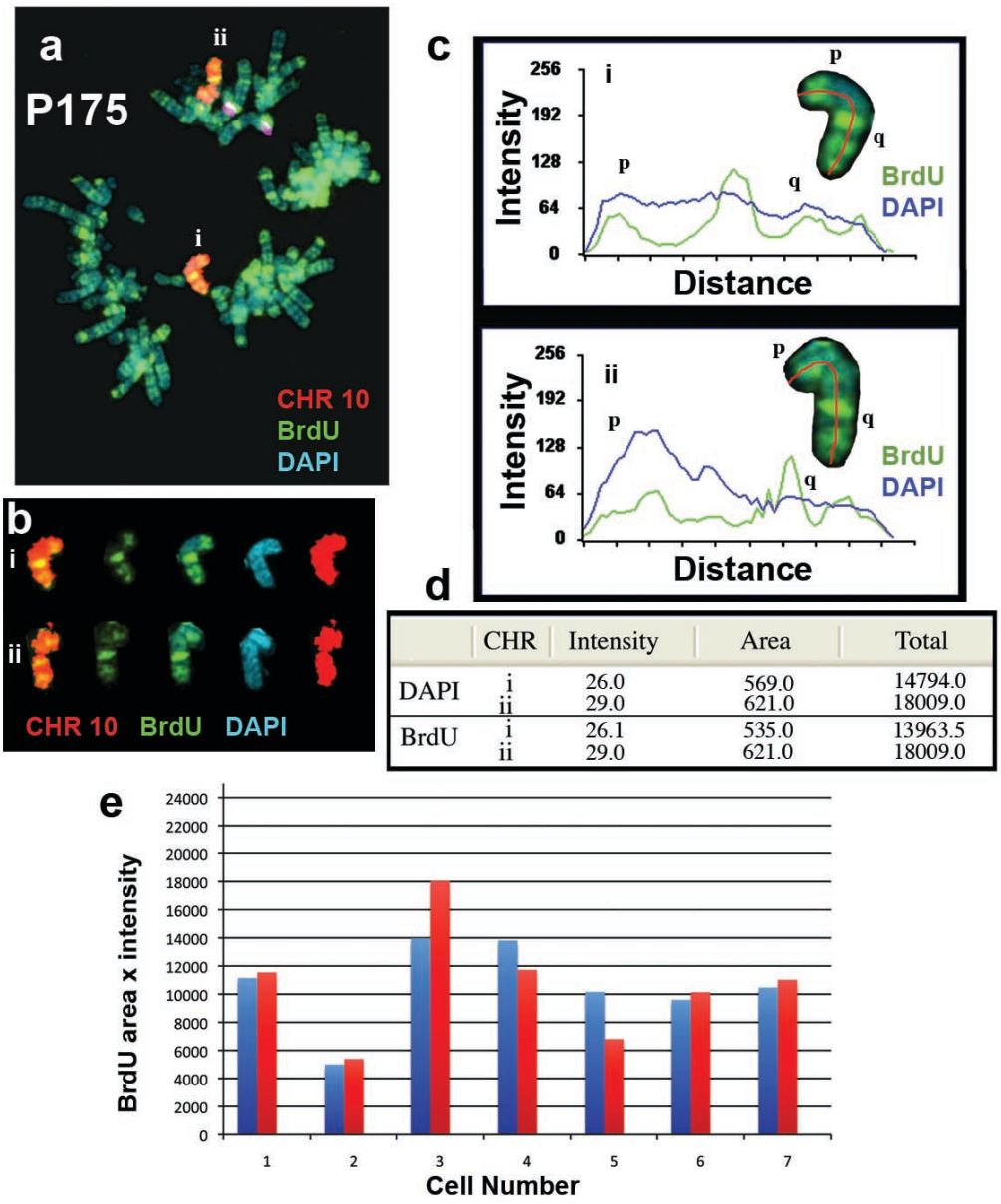

	CHR	Intensity	Area	Total
DAPI	i	26.0	569.0	14794.0
	ii	29.0	621.0	18009.0
BrdU	i	26.1	535.0	13963.5
	ii	29.0	621.0	18009.0

Sup. Fig. 15. Replication timing of chromosome 10 in P175 cells. A) An example of a mitotic spread processed for BrdU incorporation (green), FISH with a chromosome 10 paint as probe (red), and FISH with a chromosome 4 centromeric probe (purple). B) The two chromosome 10s, from panel A, separated from the rest of the spread and aligned with the different fluors overlaid in different combinations. C) Intensity profile for the BrdU incorporation and DAPI staining for the two chromosome 10s shown in panels A and B. The red line on the chromosomes represents the path used to quantify the position and location of the signal along the length of each chromosome, the short (p) and long (q) arms of the chromosome 10s are indicated. D) Quantification of the total amount of BrdU incorporation and DAPI staining (Total: pixel area x average intensity) for the two chromosome 10s in panels A and B. E) Total BrdU incorporation in chromosome 10 in P175 cells. The red and blue bars represent the two chromosome 10s from 7 different mitotic cells (Cell Number). The BrdU incorporation profile and quantification for chromosome 4 are not shown (see Sup. Fig. 16).

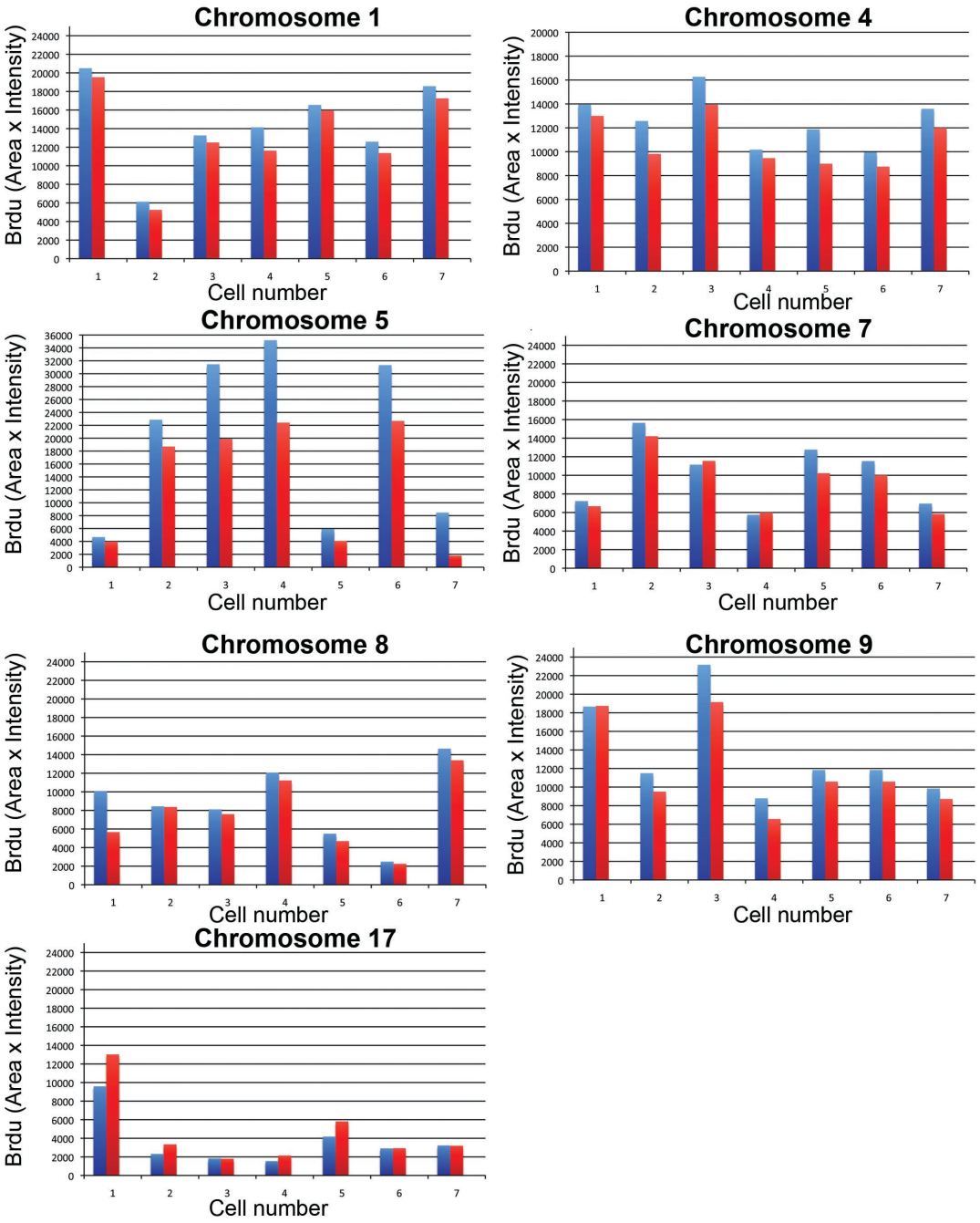

Sup. Fig. 16. Chromosome replication timing of chromosome 1, 4, 5, 7, 8, 9, and 17 in P175 cells. Each graph shows the quantification of the total amount of BrdU incorporation (BrdU Area x Intensity) for each chromosome pair. P175 cells were incubated with BrdU for 6 hours, processed for BrdU immunostaining, and subjected to FISH with chromosome-specific paints or centromeric probes. The red and blue bars represent the two homologs of the indicated chromosome pairs present in 7 different mitotic cells (Cell number).

We next assayed the chromosome replication timing of the chromosome 6 ‘alternative partner’ translocations. Cultures were incubated with BrdU for 4.5, 5 and 6 hours and mitotic cells were harvested and processed for BrdU incorporation and for FISH using a chromosome 6 paint plus centromeric probes specific to the alternative partner chromosomes, as described above. In total, DRT was detected on three of the four chromosome 6 ‘alternative partner’ translocations, a t(6;17)(q15;q25) (see Sup. Fig. 5, above), a t(6;7)(q15;q36) (see Sup. Fig. 6, above), and a t(6;9)(q15;p21) (see Fig. 1, and Sup. Fig. 8). Analysis of a fourth ‘alternative partner’ translocation involving chromosome 6, t(6;8)(q15;q24.1), indicated that it does not display DRT (see Sup. Fig. 9, above).

We next assayed the chromosome replication timing of the chromosome 10 ‘alternative partner’ translocations. Cultures were incubated with BrdU for 4.5, 5, and 6 hours and mitotic cells were harvested, and processed for BrdU incorporation and subjected to FISH using a chromosome 10 paint and chromosome-specific centromeric probes as described above. DRT was not detected on any of the three chromosome 10 ‘alternative partner’ translocations (see Sup. Figs. 10-12, above).

Engineering Deletions in Chromosome 6:

<u>Chromosome 6 Proximal Deletions:</u>

Our results obtained from the 'alternative partner' analysis suggested that the DRT phenotype segregated with the chromosome 6 loxP integration site and not with the chromosome 10 integration site in P175 cells. Therefore, we next generated internal deletions in chromosome 6, nested at the original loxP-3'RT integration site in P175 cells. First, we determine the exact location of the chromosome 6 loxP cassette insertion site using inverse PCR [11]. For this analysis, we used Southern blot hybridizations to characterize the plasmid-genome junctions of the loxP-3'RT cassette, size selected restriction fragments, circularized the fragments with ligase, and used inverse PCR with nested primers directed to the vector sequences from the loxP-3'RT cassette (data not shown). Direct sequencing of the PCR product indicated that the loxP cassette was inserted at position 96,386,321 base pairs (NCBI Build 36 version 2) of chromosome 6. This insertion site was confirmed by PCR using primers designed to amplify the plasmid-genome junctions of both the 5' and 3' ends of the inserted cassette (see Sup. Fig. 17D and Sup. Table 1). A schematic view of the loxP-3'RT insertion site, with the location of the cassette-genome junction primers, is indicated (see Sup. Fig. 17C). In addition, this analysis revealed that a 70 base pair deletion had occurred in chromosome 6 upon insertion of the original loxP-3'RT cassette (Sup. Table 1).

The rationale behind the methodology used to engineer chromosome 6 deletions was based on previous studies showing that intra-chromosomal Cre events are markedly more efficient than inter-chromosomal Cre events [reviewed

in [6]]. The design of this set of experiments was to introduce new loxP cassettes, 5'AP-loxP, into P175 cells, obtain pools of cells containing these new integration sites and subsequently transiently express Cre in each pool of clones and isolate Aprt+ colonies. Accordingly, reconstitution of the Aprt gene with Cre is expected to occur at a higher frequency in cells containing Lentiviral integrations near the original loxP-3'RT cassette. For these experiments we used a Lentiviral vector (pL6-APlox-Blas) that contains the 5' half of the Aprt gene (AP), a loxP site, and the selectable marker for Blasticidin (Blas) resistance. A schematic diagram of this Lentiviral construct is shown in (Sup. Fig. 17A, also see Fig. 2A). In addition, this virus was designed so that the Blas gene would be deleted if the virus inserted into a loxP-3'RT-containing chromosome and if it is oriented in a way that would generate a deletion following Cre-mediated recombination with the original loxP-cassette insertion site. In order to generate a large number of random integrations, we infected P175 cells with this AP-loxP-Blas virus at a multiplicity of infection of <0.1, thus insuring single copy integrations, and 45 independent pools, each containing ~5000-10,000 Blasticidin resistant colonies, were isolated. Note that with this number of pools and integration sites a new loxP cassette is predicted to be introduced throughout the P175 genome approximately every 20 kb. Subsequently, each pool was transiently transfected with a Cre expression vector, selected for reconstitution of Aprt, and independent Aprt+ clones isolated (>1,000 total clones). Due to random integration of the Lentivirus, only 1 in 4 integrations in chromosome 6 would contain the Lentivirus

in the correct position and orientation to generate deletions proximal to the original loxP-3'RT integration site. Therefore, each Aprt+ clone was tested for growth in media containing Blasticidin, and all Blasiticidin sensitive clones were expanded and analyzed by Southern blot hybridization for retention of the Blas gene and for novel Lentiviral integrations. Supplementary Figure 17B shows an example of this analysis for clones isolated from pools #1, #2, #3, #4, #5, and #6. Note that most of the Blasticidin sensitive clones have lost the Blas gene as judged by probing the blot with a Blas probe. Furthermore, probing a second blot with the 5' portion of the Aprt gene (AP probe) indicated that some of the clones from each pool retained restriction fragments of similar size, i.e. clones Δ175-1a, -1b, -1c, -1d, -1e, -1f, and -1i, suggesting that they came from the same Lentiviral integration site in Pool #1, and therefore represent the same deletion. In addition, other clones from each pool retain different size AP restriction fragments, i.e. clones Δ175-1g and -1h, indicating that these clones came from a different Lentiviral integration in Pool #1 and therefore represent different deletions. To confirm that the Blas negative clones contain deletions in chromosome 6 proximal to the original loxP-3'RT insertion site, we carried out PCR analysis with primers directed to the cassette-genome junctions. The primers were designed to detect either proximal or distal junction fragments at the original loxP-3'RT insertion site (Sup. Fig. 17C).

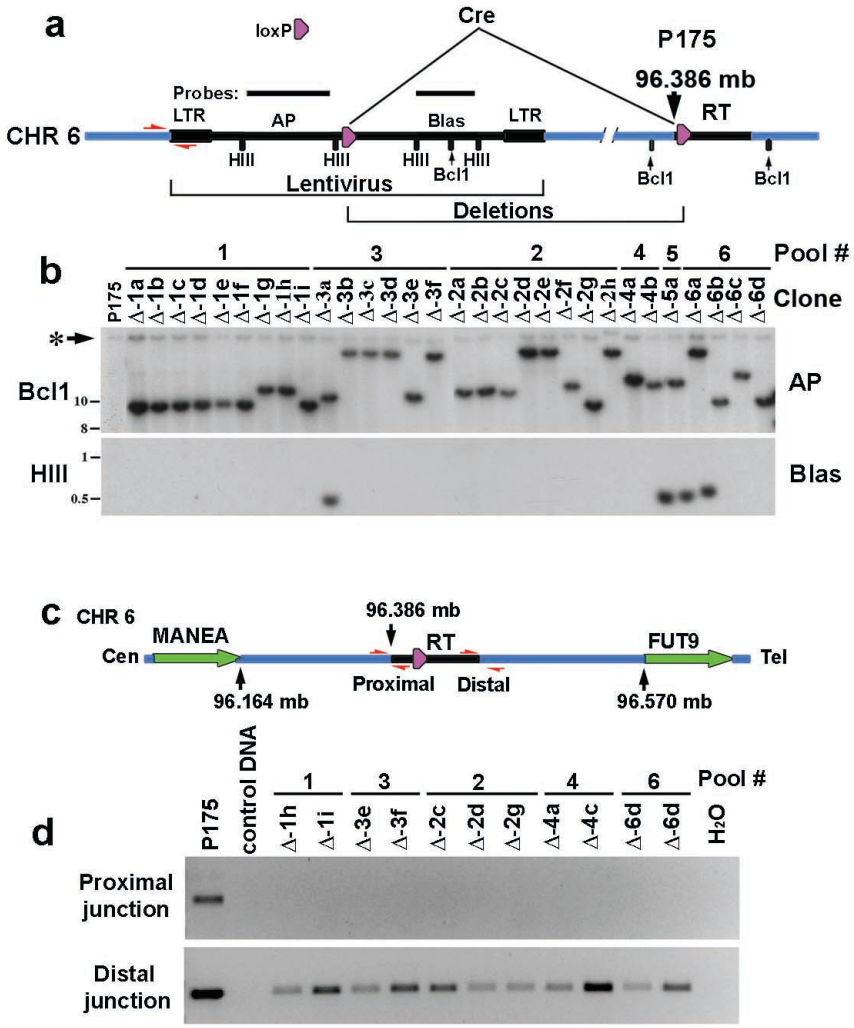

Sup. Fig. 17. Chromosome 6 proximal deletions. A). Schematic diagram of the Lentiviral vector (AP-loxP-blas) and the loxP-3'RT integration site in chromosome 6 of P175. Note that integration of the Lentivirus in the correct region and orientation will result in a Cre-dependent loss of the Blas gene. An idealized location of LTR-genome junction PCR primers (red arrows) are indicated. The Bcl1 and HindIII (HIII) sites are indicated. The original loxP-3'RT band is indicated (*). B) Southern blot hybridizations showing similar and independent Lentiviral integrations in clones from different pools of infected P175 cells, and the lack of the Blas gene in most of the Aprt+ clones. The top panel shows a blot (Bcl1 digestion) hybridized with the AP probe (see panel A), and the bottom panel shows a blot (HindIII digestion) hybridized with the Blas probe. C) Schematic view of the original loxP-3'RT integration site in P175. The integration site was determined by inverse PCR and is located at 96,386,392. The approximate location of the cassette-genome junction-PCR primers (red arrows) are indicated for both the proximal and distal junctions. D) Junction PCR for the detection of deletions. Individual Aprt+ clones isolated from the indicated pools (#1, #2, #3, #4, and #6) were subjected to PCR reactions with the proximal and distal junction-PCR primers (panel C). Note that all of the clones have lost the proximal junction but retain the distal junction.

Supplementary Figure 17D shows this analysis for a subset of clones from Pool #1, #2, #3, #4, and #6, and indicates that, as expected, the distal junction is present in all of these clones and that the proximal junction is not. In total, we have isolated P175 sub-clones that contain >40 distinct Lentiviral integrations that have lost the Blas gene and this proximal cassette-genome junction.

Chromosome 6 Distal Deletions:

One caveat to the relatively straightforward generation of deletions in chromosome 6, nested at the loxP-3'RT integration site, is that deletions could be easily generated in only one direction, i.e. proximally, from this integration site. Therefore, to generate deletions distal to the loxP-3'RT integration site, we used a second site-specific recombinase system, Flp/FRT, to engineer deletions distal to the loxP-3'RT cassette in chromosome 6 of P175 cells. Like Cre, the Flp recombinase can be used in combination with its recognition sequence, FRT, to generate site-specific rearrangements in mammalian chromosomes [(1)]. For these experiments we first integrated a plasmid containing a single loxP site located in the second intron of an AP-loxP cassette (Sup. Fig. 18). Thus, in a Cre-dependent manner this plasmid is directed to the original loxP-3'RT integration site in chromosome 6 of P175, and properly targeted integrations are recovered by selection for reconstitution of the Aprt gene. The integrated plasmid also contained a second 3'RT cassette (positioned in the opposite orientation from the

original cassette) linked to an FRT site in its second intron. The integration plasmid also contained a second FRT site located 5' of the AP cassette in the configuration shown in Sup. Fig. 18.

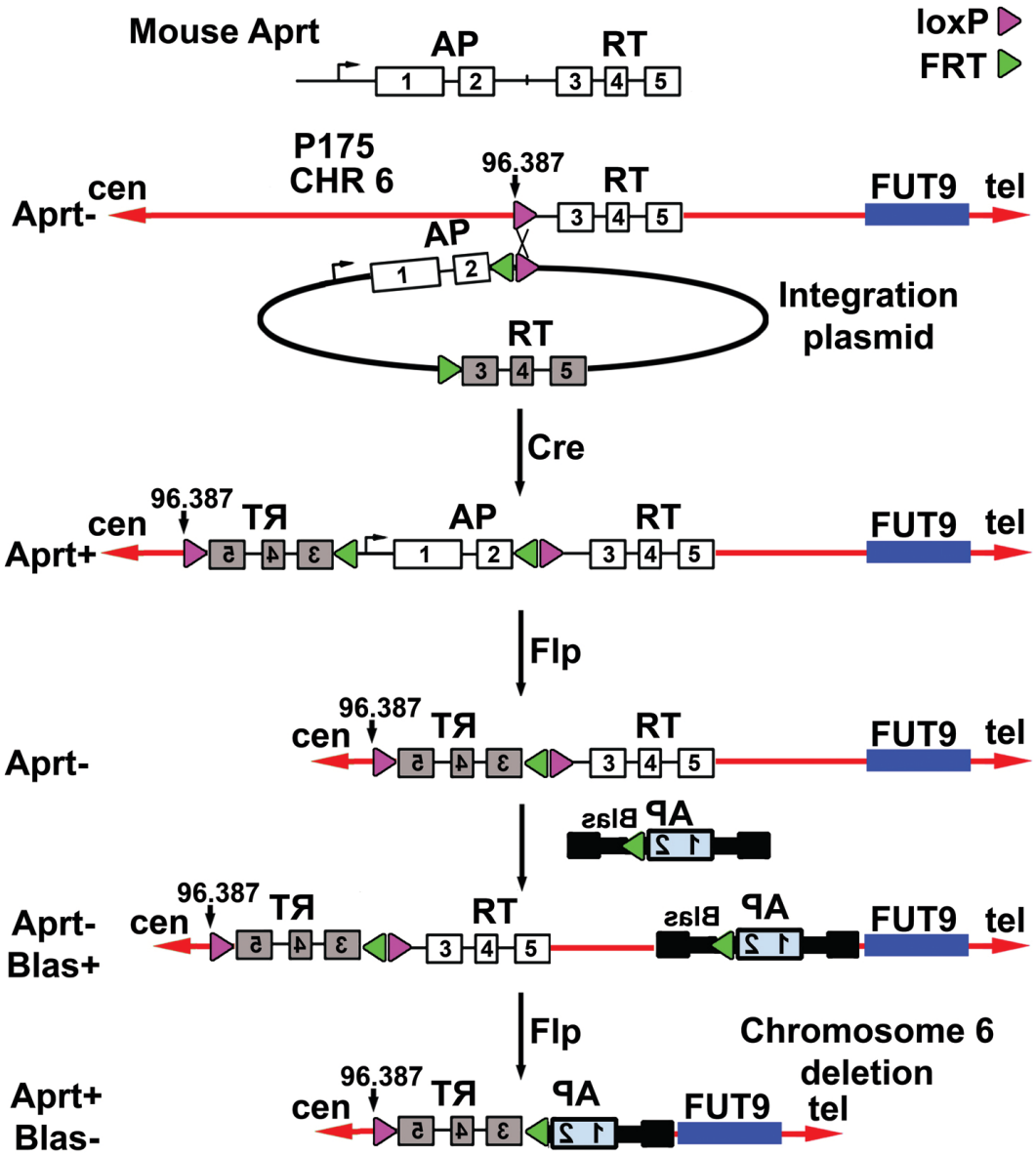

Sup. Fig. 18. Engineering scheme for chromosome 6 distal deletions. Schematic diagram of the mouse Aprt gene, the location and orientation of the original loxP-3'RT site, the 'integration' plasmid (containing a single loxP site and an FRT-RT cassette, the Lentiviral vector (L6-AP-FRT-Blas, in reverse in black), and Flp-mediated deletion and reconstitution of APRT. Note that integration of the Lentivirus in the correct region and orientation will result in a Flp-dependent loss of the Blas gene in the final step.

This strategy allowed us to remove the AP portion of the integrated plasmid by transient expression of Flp, which allowed us to re-isolated Aprt- cells and to reuse the Aprt selectable marker. Subsequently, these Aprt- cells were infected with a Lentivirus (L6-AP-FRT-Blas) containing an AP-FRT cassette, as shown (Sup. Fig. 18), and pools of Blasticidin-resistant colonies were isolated and transiently transfected with a Flp expression vector followed by the re-isolation of Aprt+ colonies.

Using the same strategy that we used to identify and characterize the proximal deletions in chromosome 6, described above (Sup. Fig. 17), we isolated four Flp/FRT-mediated deletions in chromosome 6 distal to the original loxP-3'RT integration site, ranging in size from ~26 mb to as small as ~18 kb (see Sup. Table 1 and Sup. Fig. 19).

We next used LAM-PCR [12] to clone and sequence the Lentiviral integration sites in a subset of these deletion clones. LAM-PCR was performed using primers directed at the 5' LTR, and was carried out at the Fred Hutchinson Cancer Research Center's Clonal Analysis Core facility (http://www.fhcrc.org/science/shared_resources/cceh-clonal/index.html). We have successfully cloned and sequenced LAM-PCR products from 21 of the >50 Lentiviral integrations (Sup. Table 1). In addition, we have confirmed all 21 integration sites using PCR with primers (see Sup. Table 3) directed at the Lentiviral 5'LTR-genome junction sites (not shown). Furthermore, we have confirmed that these 21 different Lentiviral integration sites generated deletions

in chromosome 6 using LOH analysis (see below) and FISH with probes representing BAC RP11-374I15 (see Fig. 2 and Sup. Fig. 23), BAC CTD-2231M1 (see Sup. Figs. 19, 25A and 25B) or with Fosmid G248P86031E7 (see Fig. 2A and 3F).

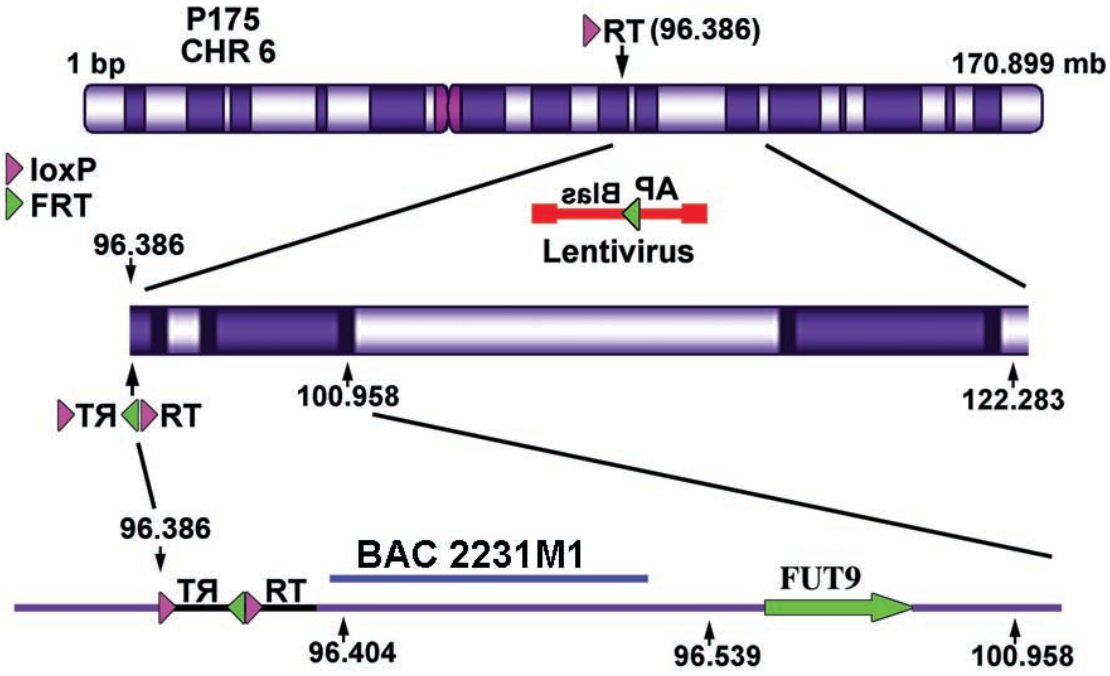

Sup. Fig. 19. Chromosome 6 deletions distal to the loxP-3'RT site in chromosome 6. Schematic diagram of chromosome 6 in P175 cells showing the integration plasmid at the original loxP-3'RT integration site, the location of BAC CTD-2231M1, the Lentiviral vector (L6-AP-FRT-blas; in the reverse orientation), and the Lentiviral integration sites along chromosome 6 (arrows, numbers are in megabases; also see Sup. Table 1). Note that integration of a Lentivirus only in the correct region and orientation will result in Cre-dependent loss of the Blas gene.

Affymetrix Genotyping, Copy Number, and Loss of Heterozygosity:

In order to characterize these chromosome 6 deletions in molecular detail, we have carried out a genotyping and copy number analysis of the parental cell lines

HTD114 and P175 and two different clones containing proximal deletions in chromosome 6, Δ175-2d (~16.6 mb deletion) and Δ175-1i (~231 kb deletion) using the Affymetrix 500K SNP array. The array hybridizations were subjected to a performance evaluation. The metrics that were used for this evaluation were those suggested by Affymetrix, Inc. The quality of the hybridizations were assessed using two sets of measurements: 1) the genotype call rates across the array as determined by the Affymetrix Dynamic Modeling (DM) algorithm and 2) pair-wise comparison of the genotypes from 50 SNPs that are tiled onto both the NspI and the StyI arrays. Passing call rates suggested by Affymetrix are >93%. The call rates for our initial analyses were 95.84% for the Nsp1 array and 95.33% for the Sty1 array. In addition, the OHSU Affymetrix core uses 48 identical calls out of the 50 common SNPs (96%) as a passing threshold. Our analysis yielded 50 out of 50 identical calls on all samples.

In order to characterize the extent of the deletions in chromosome 6, present in the Δ175-2d and Δ175-1i cell lines, we carried out loss of heterozygosity (LOH) and copy number analyses, using the micro-array SNP data and Partek Genomics Suite software. Supplementary Figures 20 and 21 show the results of this analysis and indicate that both cell lines contain LOH and decreased copy number at the chromosomal positions predicted by the two integrated loxP cassettes in each clone. For example, the original loxP-3'RT integration in P175 is at position 96,386,321 and in both deletion cell lines LOH begins at the first heterozygous SNP proximal to this integration site.

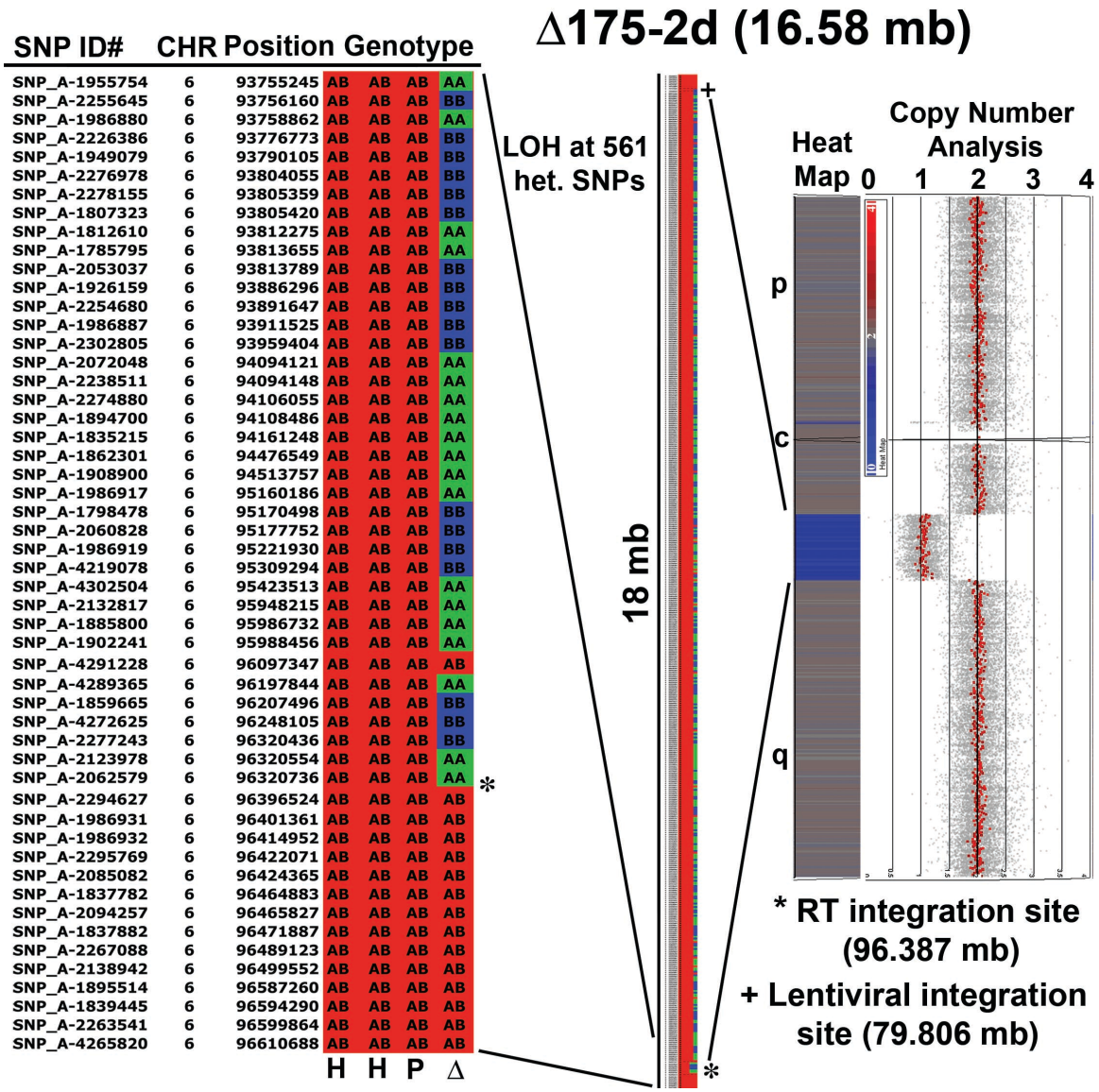

SNP ID#	CHR	Position	Genotype			
SNP_A-1955754	6	93755245	AB	AB	AB	AA
SNP_A-2255645	6	93756160	AB	AB	AB	BB
SNP_A-1986880	6	93758862	AB	AB	AB	AA
SNP_A-2226386	6	93776773	AB	AB	AB	BB
SNP_A-1949079	6	93790105	AB	AB	AB	BB
SNP_A-2276978	6	93804055	AB	AB	AB	BB
SNP_A-2278155	6	93805359	AB	AB	AB	BB
SNP_A-1807323	6	93805420	AB	AB	AB	BB
SNP_A-1812610	6	93812275	AB	AB	AB	AA
SNP_A-1785795	6	93813655	AB	AB	AB	AA
SNP_A-2053037	6	93813789	AB	AB	AB	BB
SNP_A-1926159	6	93886296	AB	AB	AB	BB
SNP_A-2254680	6	93891647	AB	AB	AB	BB
SNP_A-1986887	6	93911525	AB	AB	AB	BB
SNP_A-2302805	6	93959404	AB	AB	AB	BB
SNP_A-2072048	6	94094121	AB	AB	AB	AA
SNP_A-2238511	6	94094148	AB	AB	AB	AA
SNP_A-2274880	6	94106055	AB	AB	AB	AA
SNP_A-1894700	6	94108486	AB	AB	AB	AA
SNP_A-1835215	6	94161248	AB	AB	AB	AA
SNP_A-1862301	6	94476549	AB	AB	AB	AA
SNP_A-1908900	6	94513757	AB	AB	AB	AA
SNP_A-1986917	6	95160186	AB	AB	AB	AA
SNP_A-1798478	6	95170498	AB	AB	AB	BB
SNP_A-2060828	6	95177752	AB	AB	AB	BB
SNP_A-1986919	6	95221930	AB	AB	AB	BB
SNP_A-4219078	6	95309294	AB	AB	AB	BB
SNP_A-4302504	6	95423513	AB	AB	AB	AA
SNP_A-2132817	6	95948215	AB	AB	AB	AA
SNP_A-1885800	6	95986732	AB	AB	AB	AA
SNP_A-1902241	6	95988456	AB	AB	AB	AA
SNP_A-4291228	6	96097347	AB	AB	AB	AB
SNP_A-4289365	6	96197844	AB	AB	AB	AA
SNP_A-1859665	6	96207496	AB	AB	AB	BB
SNP_A-4272625	6	96248105	AB	AB	AB	BB
SNP_A-2277243	6	96320436	AB	AB	AB	BB
SNP_A-2123978	6	96320554	AB	AB	AB	AA
SNP_A-2062579	6	96320736	AB	AB	AB	AA
SNP_A-2294627	6	96396524	AB	AB	AB	AB
SNP_A-1986931	6	96401361	AB	AB	AB	AB
SNP_A-1986932	6	96414952	AB	AB	AB	AB
SNP_A-2295769	6	96422071	AB	AB	AB	AB
SNP_A-2085082	6	96424365	AB	AB	AB	AB
SNP_A-1837782	6	96464883	AB	AB	AB	AB
SNP_A-2094257	6	96465827	AB	AB	AB	AB
SNP_A-1837882	6	96471887	AB	AB	AB	AB
SNP_A-2267088	6	96489123	AB	AB	AB	AB
SNP_A-2138942	6	96499552	AB	AB	AB	AB
SNP_A-1895514	6	96587260	AB	AB	AB	AB
SNP_A-1839445	6	96594290	AB	AB	AB	AB
SNP_A-2263541	6	96599864	AB	AB	AB	AB
SNP_A-4265820	6	96610688	AB	AB	AB	AB

Sup. Fig. 20. SNP analysis of a chromosome 6 deletion. Affymetrix 500K SNP arrays were performed on two independent isolates of genomic DNA from the starting cell line HTD114 (H), and single genomic DNA isolates of P175 (P) and Δ175-2d (Δ). Δ175-2d is predicted to have an ~16.58 megabase deletion, based on the LAM-PCR integration site (Sup. Table 1). The left and middle panels show the heterozygous SNPs, defined as AB calls in both runs of the HTD114 DNA, comparing HTD114 to P175 and Δ175-2d. The genotype calls were imported into Excel and color-coded, with the AA genotype in green, the BB genotype in blue, and the AB genotype in red. The SNP ID#, chromosome (CHR), position and genotype calls are indicated. The middle panel shows an ~18 megabase region of chromosome 6, and the left panel shows an expanded view of this region. The genomic locations of the original loxP-3'RT and Lentiviral integration sites are shown (* and +, respectively). The right panel shows the copy number and Heat Map analysis for a pair-wise comparison between P175 and Δ175-2d for chromosome 6. The positions of the short (p) and long (q) arms, as well as the centromere (c) are indicated.

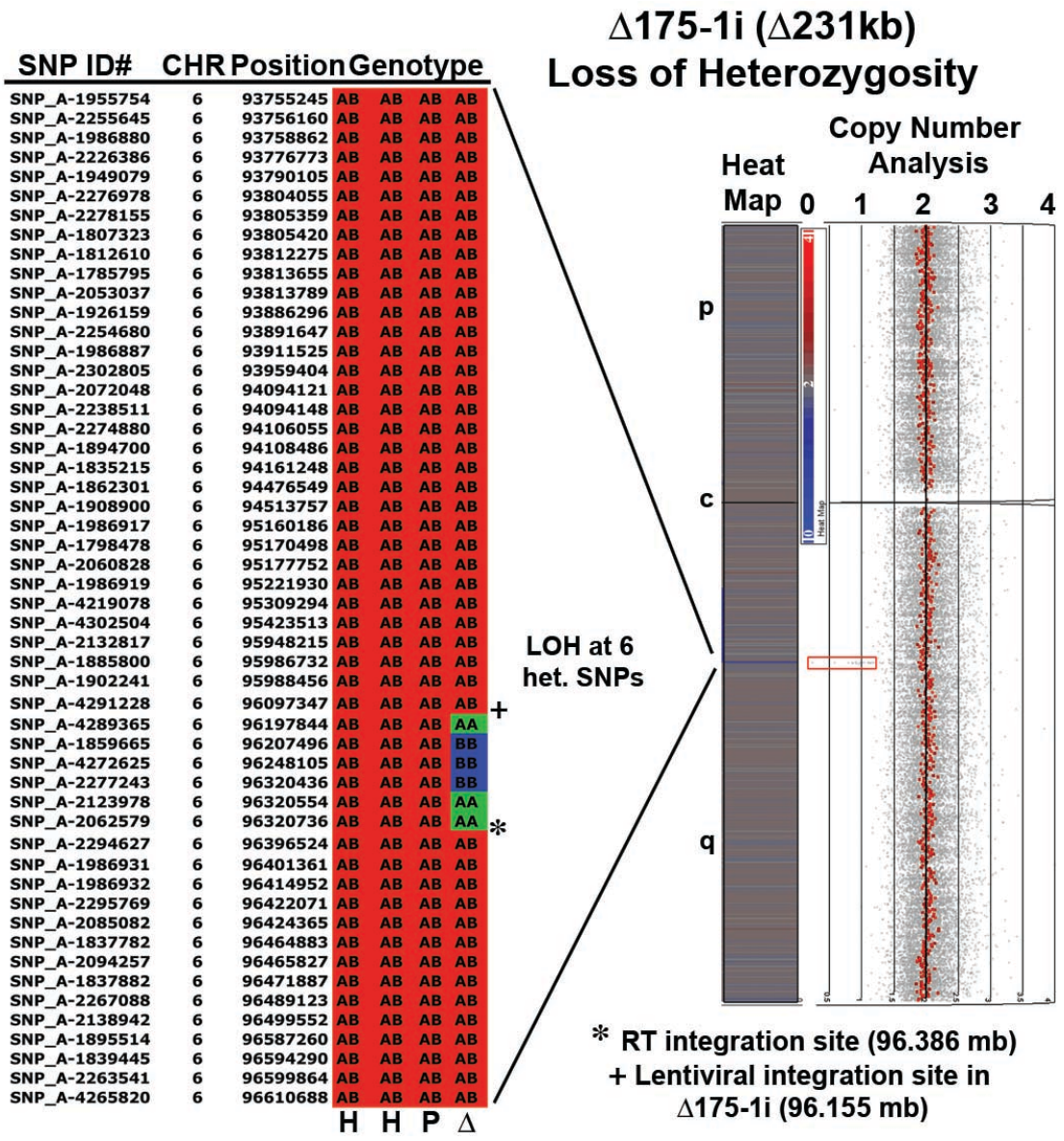

SNP ID#	CHR	Position	H	H	P	Δ	
SNP_A-1955754	6	93755245	AB	AB	AB	AB	
SNP_A-2255645	6	93756160	AB	AB	AB	AB	
SNP_A-1986880	6	93758862	AB	AB	AB	AB	
SNP_A-2226386	6	93776773	AB	AB	AB	AB	
SNP_A-1949079	6	93790105	AB	AB	AB	AB	
SNP_A-2276978	6	93804055	AB	AB	AB	AB	
SNP_A-2278155	6	93805359	AB	AB	AB	AB	
SNP_A-1807323	6	93805420	AB	AB	AB	AB	
SNP_A-1812610	6	93812275	AB	AB	AB	AB	
SNP_A-1785795	6	93813655	AB	AB	AB	AB	
SNP_A-2053037	6	93813789	AB	AB	AB	AB	
SNP_A-1926159	6	93886296	AB	AB	AB	AB	
SNP_A-2254680	6	93891647	AB	AB	AB	AB	
SNP_A-1986887	6	93911525	AB	AB	AB	AB	
SNP_A-2302805	6	93959404	AB	AB	AB	AB	
SNP_A-2072048	6	94094121	AB	AB	AB	AB	
SNP_A-2238511	6	94094148	AB	AB	AB	AB	
SNP_A-2274880	6	94106055	AB	AB	AB	AB	
SNP_A-1894700	6	94108486	AB	AB	AB	AB	
SNP_A-1835215	6	94161248	AB	AB	AB	AB	
SNP_A-1862301	6	94476549	AB	AB	AB	AB	
SNP_A-1908900	6	94513757	AB	AB	AB	AB	
SNP_A-1986917	6	95160186	AB	AB	AB	AB	
SNP_A-1798478	6	95170498	AB	AB	AB	AB	
SNP_A-2060828	6	95177752	AB	AB	AB	AB	
SNP_A-1986919	6	95221930	AB	AB	AB	AB	
SNP_A-4219078	6	95309294	AB	AB	AB	AB	
SNP_A-4302504	6	95423513	AB	AB	AB	AB	
SNP_A-2132817	6	95948215	AB	AB	AB	AB	
SNP_A-1885800	6	95986732	AB	AB	AB	AB	
SNP_A-1902241	6	95988456	AB	AB	AB	AB	
SNP_A-4291228	6	96097347	AB	AB	AB	AB	+
SNP_A-4289365	6	96197844	AB	AB	AB	AA	
SNP_A-1859665	6	96207496	AB	AB	AB	BB	
SNP_A-4272625	6	96248105	AB	AB	AB	BB	
SNP_A-2277243	6	96320436	AB	AB	AB	BB	
SNP_A-2123978	6	96320554	AB	AB	AB	AA	
SNP_A-2062579	6	96320736	AB	AB	AB	AA	*
SNP_A-2294627	6	96396524	AB	AB	AB	AB	
SNP_A-1986931	6	96401361	AB	AB	AB	AB	
SNP_A-1986932	6	96414952	AB	AB	AB	AB	
SNP_A-2295769	6	96422071	AB	AB	AB	AB	
SNP_A-2085082	6	96424365	AB	AB	AB	AB	
SNP_A-1837782	6	96464883	AB	AB	AB	AB	
SNP_A-2094257	6	96465827	AB	AB	AB	AB	
SNP_A-1837882	6	96471887	AB	AB	AB	AB	
SNP_A-2267088	6	96489123	AB	AB	AB	AB	
SNP_A-2138942	6	96499552	AB	AB	AB	AB	
SNP_A-1895514	6	96587260	AB	AB	AB	AB	
SNP_A-1839445	6	96594290	AB	AB	AB	AB	
SNP_A-2263541	6	96599864	AB	AB	AB	AB	
SNP_A-4265820	6	96610688	AB	AB	AB	AB	

Sup. Fig. 21. SNP analysis of chromosome 6 deletions. Affymetrix 500K SNP arrays were performed on two independent isolates of genomic DNA from the starting cell line HTD114 (H), and single genomic DNA isolates of P175 (P) and Δ175-1i (Δ). Δ175-1i is predicted to have an ~231 kb deletion. The left panel shows the heterozygous SNPs, defined as AB calls in both runs of the HTD114 DNA, comparing the genotype of HTD114 to P175 and Δ175-1i. The genotype calls were imported into Excel and color-coded, with the AA genotype in green, the BB genotype in blue, and the AB genotype in red. The SNP ID#, chromosome (CHR), position and genotype calls are indicated. The left panel shows an ~2.8 mb region of chromosome 6. The genomic locations of the original loxP-3'RT and Lentiviral integration sites are shown (* and +, respectively). The right panel shows the copy number and Heat Map analysis for a pair-wise comparison between P175 and Δ175-1i for chromosome 6. The positions of the short (p) and long (q) arms, as well as the centromere (c) are indicated. The red box highlights the region of chromosome 6 that shows decreased copy number and loss of heterozygosity.

In addition, the LOH continues in each cell line until the first heterozygous SNP proximal to the Lentiviral integration site for each clone (Sup. Figs. 20 and 21, and see Sup. Table 1). Similarly, we find decreased copy number at the same genomic positions as observed in the LOH analysis for each cell line (Sup. Figs. 20 and 21). Finally, using PCR and sequencing, we have confirmed >100 of these heterozygous SNPs, located on chromosomes 6, 10, 13, and 15 (see Figs. 4B, 4C, 5B and Sup. Table 2, and not shown). In total, we have identified >119,000 heterozygous SNPs located throughout the genome of the HTD114 cell line, from which all of the chromosome rearrangements described in this study were generated. In addition, we have identified heterozygous SNPs that reside within the chromosome 6 deleted regions (see Sup. Figs. 20 and 21). Subsequent PCR and sequencing of the heterozygous SNPs located within the deleted regions, confirmed that all of the deletion lines generated here have indeed lost heterozygosity either proximal or distal to the loxP-3'RT integration site and retained heterozygosity in the opposite orientation (not shown). In addition, we have determined which SNP alleles are associated with the loxP-3'RT insertion site in P175 by PCR and sequencing from DNA isolated from mono-chromosomal hybrids containing the individual chromosome 6s (see Sup. Table 2). These data indicate that we have generated a set of nested deletions anchored at the original loxP-3'RT integration site in chromosome 6 of P175, and that the proximal deletions range in size from ~30 mb down to ~76 kb (see Sup.

Table 1 and Fig. 2A), and that the distal deletions range in size from ~26 mb down to ~18kb (see Sup. Table 1 and Sup. Fig. 19).

Replication timing of chromosome 6 deletions.

We next assayed the replication timing of the chromosome 6s in a subset of these deletion clones. Cultures were incubated with BrdU for 4.5 hours and mitotic cells were harvested, processed for BrdU incorporation and subjected to FISH using chromosome 6-specific probes. For all of the deletion clones assayed, we first used FISH with a chromosome 6-specific paint in conjunction with the BrdU incorporation. This analysis allowed us to visualize all of the chromosome 6 material present in every cell. This was important as chromosomes with DRT/DMC are unstable and frequently participate in secondary rearrangements [(2)]. Thus, the paints allowed us to assay cells in which additional rearrangements in chromosome 6 were not present, for examples of this assay see Sup. Figs. 3, 13, 14, 15, 22 and 24. However, this assay did not allow us to unambiguously identify the deleted chromosomes. Therefore, we also combined the BrdU incorporation assay with FISH using a chromosome 6 centromeric probe plus a BAC or Fosmid from the deleted regions (see Fig. 2A and Sup. Fig. 19) on mitotic preparations containing intact chromosomes as judged by the chromosome paints, assayed above. The FISH signal from the chromosome 6 centromeric probe allowed us to identify both chromosome 6s,

and the presence or absence of the BAC/Fosmid allowed us to distinguish between the non-deleted or deleted chromosomes, respectively. Comparing the BrdU incorporation pattern of the deleted chromosome 6s to the non-deleted chromosome 6s indicated that the deleted chromosomes present in Δ175-2c (~21.8 mb deletion; Sup. Fig. 22), Δ175-2g (~2.1 mb deletion; not shown), Δ175-3e (~235 kb deletion, not shown), Δ175-1i (~232 kb deletion; Sup. Fig. 23), Δ175-11d (~96 kb deletion; Sup. Fig. 24) were delayed in replication timing by at least 2 hours. In addition, analysis of cells containing the smallest chromosome 6 proximal deletion, (~76 kb deletion) present in the Δ175-23a cell line, indicated that the deleted chromosome was delayed in replication timing by >2 hours (Fig. 3).

We next assayed the replication timing of the chromosome 6s containing deletions distal to the original loxP-3'RT integration site. Supplementary Figure 25 shows the BrdU incorporation analysis, combined with FISH using a chromosome 6 centromeric probe plus BAC CTD-2231M1 (see Sup. Fig. 19), for three independent deletions, and indicates that chromosomes containing deletions of ~25.9 mb (A-C), ~1.4 mb (D), and ~17 kb (E) did not display DRT.

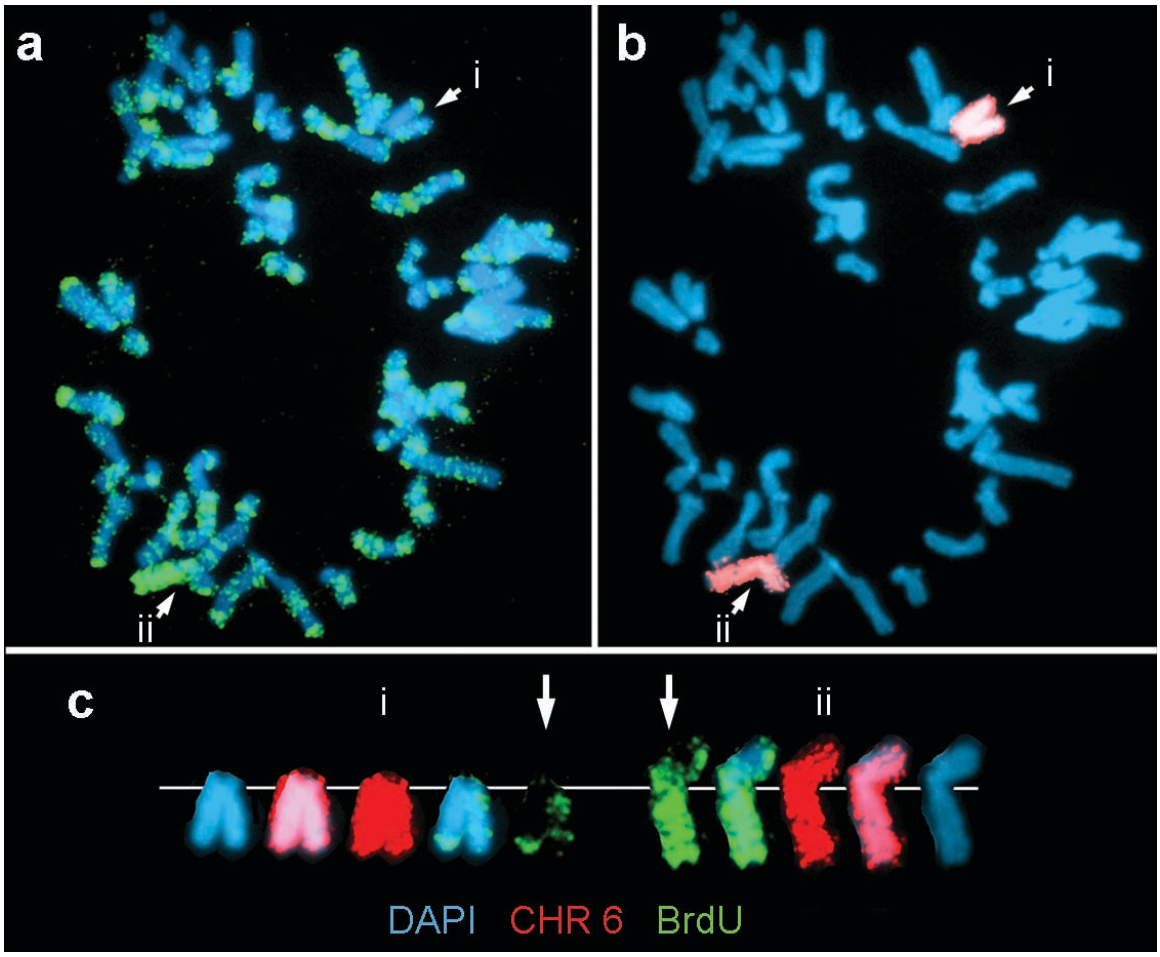

Sup. Fig. 22. Replication timing assay for chromosome 6 in Δ175-2c (~21.9 mb deletion). Cells were incubated with BrdU for 4.5 hours followed by mitotic chromosome harvest. Fixed cells were dropped on microscope slides and processed for FISH using a chromosome 6 paint (red), stained for BrdU incorporation (green), and counterstained with DAPI (blue). A and B) Mitotic chromosome spread showing the two chromosome 6s (i and ii), BrdU incorporation (green in panels A and C) and chromosome 6 paint (red in panels B and C). C) The two chromosome 6s from the same cell as in A and B, are aligned with their centromeres positioned on a white line. The arrows mark the FITC signal from the BrdU incorporation for comparison.

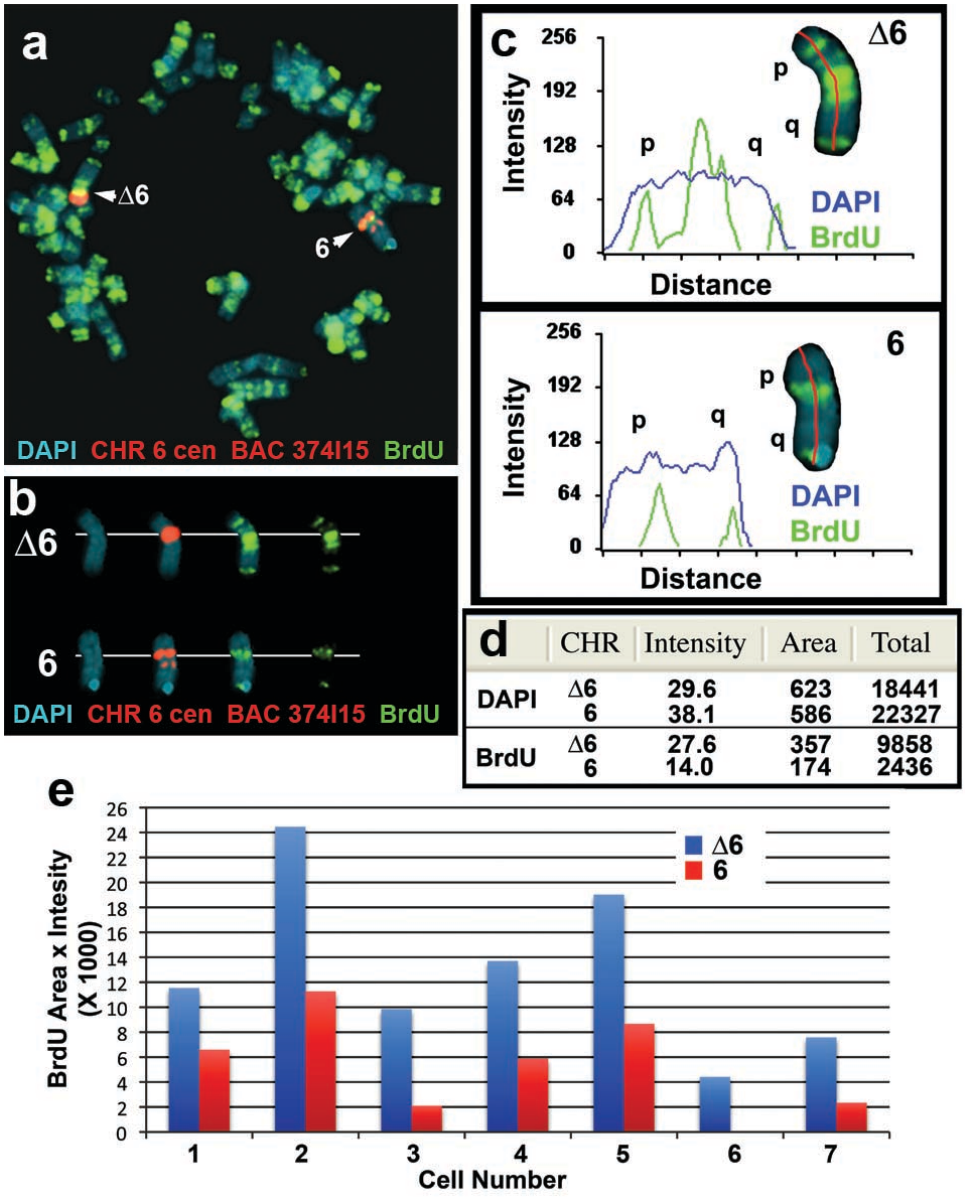

Sup. Fig. 23. Replication timing of chromosome 6 in Δ175-1i cells (~231 kb deletion). A) An example of a mitotic spread processed for BrdU incorporation (green) and FISH with chromosome 6 centromere (red) and BAC3741I5 (red) probes. The deleted chromosome 6 (Δ6) lacks the BAC signal. B) The two chromosome 6s were separated from the rest of the spread and the different fluors were overlaid in different combinations. C) Intensity profile of the BrdU incorporation and DAPI staining for the two chromosome 6s shown in panels A and B. The red line on each chromosome represents the path, starting on the short arm, used to determine the distance and location of the signal along the length of each chromosome, the short (p) and long (q) arms of the chromosome 6s. D) Quantification of the total amount of BrdU incorporation and DAPI staining for the two chromosome 6s shown in panels A-C. The values represent pixels. E) Total BrdU incorporation in the chromosome 6s in Δ175-1i cells. The red (6) and blue (Δ6) bars represent the two chromosome 6s from 7 different mitotic cells (Cell Number).

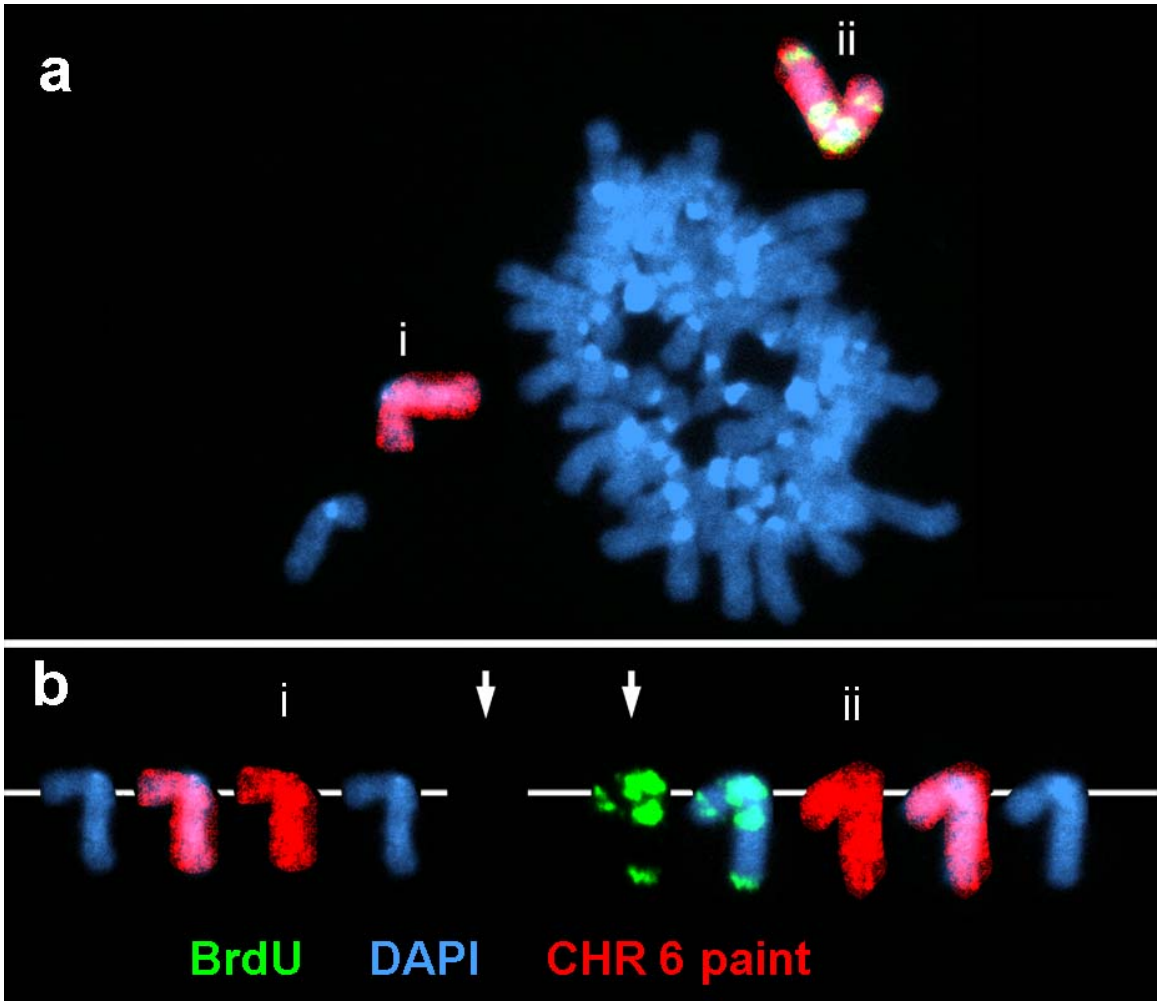

Sup. Fig. 24. Replication timing assay for chromosome 6 in Δ175-11d (~94kb deletion). Cells were incubated with BrdU for 4.5 hours followed by mitotic chromosome harvest. A) Mitotic chromosome spread showing the two chromosome 6s (i and ii), BrdU incorporation (green) and chromosome 6 paint (red). B) The two chromosome 6s from the same cell as in A, are aligned with their centromeres positioned on a white line with the different flours in different combinations. Arrows mark the BrdU only signal from both chromosomes for comparison.

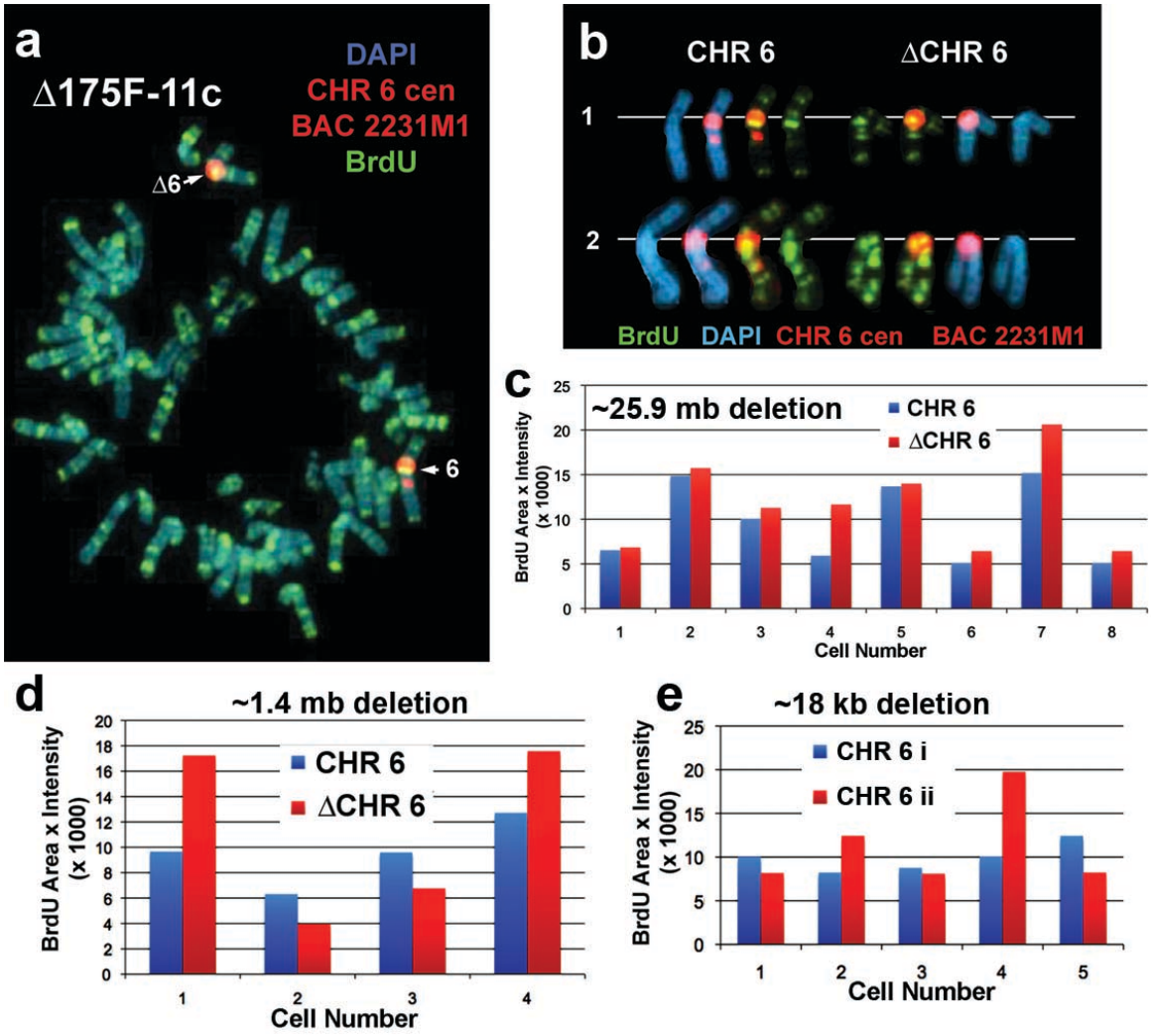

Sup. Fig. 25. Replication timing of chromosome 6 in the distal deletion lines. A) An example of a mitotic spread from Δ175F-11c (~25.9 mb deletion) processed for BrdU incorporation (green) and FISH with chromosome 6 centromere (red) and BAC CTD-2231M1 (red) probes. The deleted chromosome 6 (Δ6) lacks the BAC signal. B) The two chromosome 6s from two different mitotic cells were separated from the rest of the spread and the different fluors were overlaid in different combinations. C-E) Total BrdU incorporation in the chromosome 6s in Δ175F-11c (~25.9 mb deletion), Δ175F-11a (1.4 mb deletion) and Δ175F-7a cells (C, D, and E, respectively). The red (6) and blue (Δ6) bars represent the two chromosome 6s from different mitotic cells (Cell Number).

Characterization and Mono-allelic expression of FHLOST

We also attempted to determined if the FHL5 gene was mono-allelic in our cell system. For this analysis we used RT-PCR followed by sequencing of

heterozygous SNPs. We detected mono-allelic expression from within, and telomeric of, the FHL5 gene (Sup. Fig. 26, and Sup. Table 2).

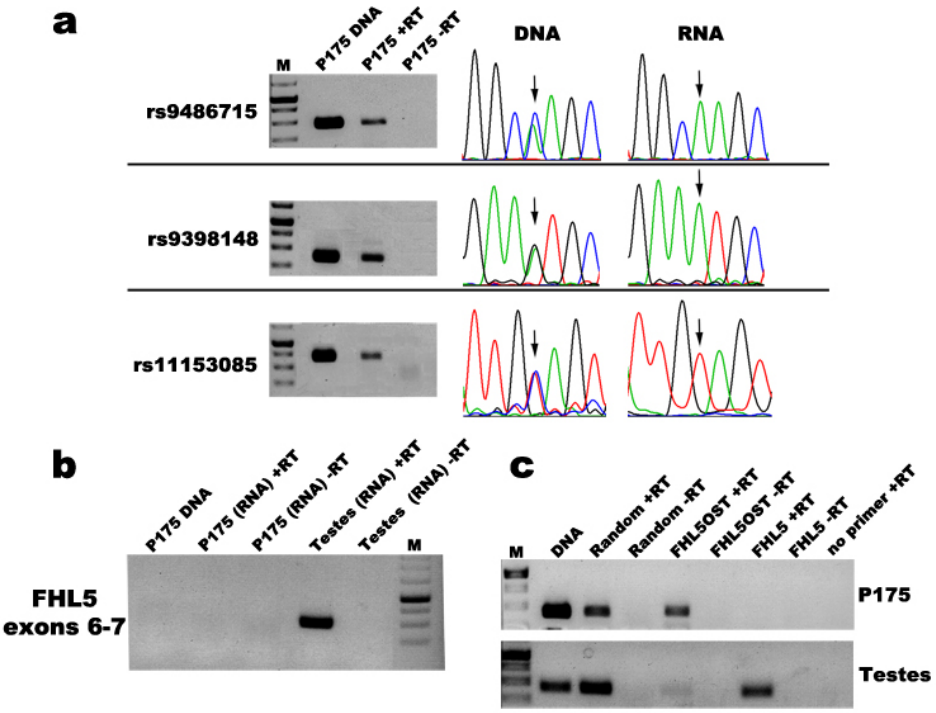

Sup. Fig. 26. Mono-allelic expression of FHL5OST. a) RT-PCR of two SNPs located within introns of FHL5, rs9486715 and rs9398148, and a SNP located telomeric to FHL5, rs11153085. PCRs were carried out on genomic DNA from P175 or RNA from P175 treated either with (+RT) or without (-RT) reverse transcriptase. Sequencing traces from the same PCR products are shown in the right panels for each SNP and each PCR. The arrows mark the locations of the heterozygous SNPs. b) Exon-specific RT-PCR for expression of FHL5. PCRs were carried out, with primers designed to detect exons 6 and 7 from the spliced FHL5 cDNA, on RNA from P175 either with (+RT) or without (-RT) reverse transcriptase. PCR on testes cDNA (+RT) yielded the correct size product, which was confirmed by sequencing (not shown). PCR products were not detected from P175 DNA, because the intron spanned by these two primers is >5 kb. Sequencing of the Testes PCR product revealed properly spliced FHL5 cDNA (not shown). c) RT-PCR products are from the FHL5 opposite strand in P175. Strand-specific reverse transcriptase reactions were carried out with primers designed to generate cDNA from either the FHL5 or FHL5-opposite strand on RNA from P175 or testes either with (+RT) or without (-RT) reverse transcriptase. Subsequent PCR with internal primers, designed to detect SNP rs94867115, indicated that the transcripts were synthesized from the opposite strand from FHL5. Both products were generated from testes RNA, which served as control for these reactions.

However, FHL5 exon-spanning primers failed to generate RT-PCR products (Sup. Fig. 26b), and these transcripts were generated in the antisense orientation

to FHL5 (Sup. Fig. 26c), indicating that the FHL5 protein-coding sequence was not expressed. We have named these FHL5 opposite strand transcripts FHL5OST.

RNA-DNA FISH for expression of ASAR6, FUT9, MANEA and FHL5OST:

We have used allele-specific RT-PCR (Fig. 4a and 5a), sequencing of RT-PCR products containing SNPs (Fig. 4b, 4c, 5b, and Sup. Table 2), RT-PCR on RNA isolated from mono-chromosomal hybrids (Fig. 4d and Sup. Table 2), and RNA-DNA FISH (Fig. 4f, 4g, 5e, 5f, and 7c-f) to examine the allelic expression of ASAR6, FUT9, MANEA and FHL5OST. Supplementary Figure 27 shows additional RNA-DNA FISH images, using three independent probes for ASAR6, on a panel of single nuclei from P175 cells. Supplementary Figure 28 shows additional RNA-DNA FISH images, using the FUT9 cDNA as probe, on a panel of single nuclei from P175 cells. Supplementary Figure 29 shows additional RNA-DNA FISH images, using the FUT9 cDNA as probe, on a panel of single nuclei from Δ175-1i cells. Supplementary Figure 30 shows additional RNA-DNA FISH images, using the FUT9 intronic probe, on a panel of single nuclei from P175 cells. Supplementary Figure 31 shows additional RNA-DNA FISH images, using the FUT9 intronic probe, on a panel of single nuclei from Δ175-1i cells. Supplementary Figure 32 shows additional RNA-DNA FISH images, using the MANEA cDNA as probe, on a panel of single nuclei from P175 cells. Supplementary Figure 33 shows additional RNA-DNA FISH images, using the

MANEA cDNA as probe, on a panel of single nuclei from Δ175-1i cells. Supplementary Figure 34 shows RNA-DNA FISH images, for FHL5OST using Fosmid G248P86054G4, on a panel of single nuclei from P175 cells. Supplementary Figure 35 shows RNA-DNA FISH images, for FHL5OST using Fosmid G248P86054G4, on a panel of single nuclei from Δ175-1i cells.

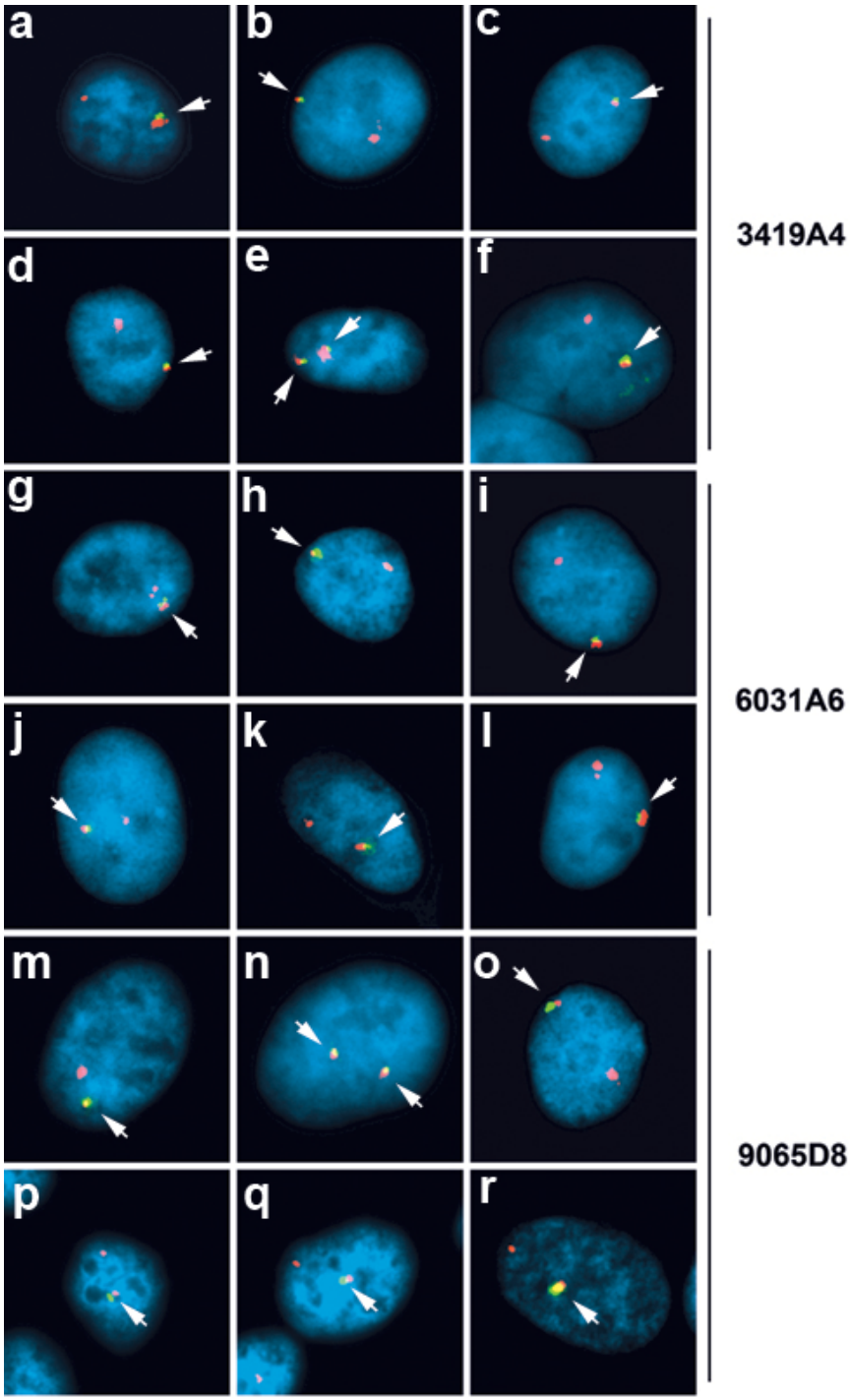

Sup. Fig. 27. RNA-DNA FISH for ASAR6. P175 cells were subjected to RNA-DNA FISH using the Fosmids G248P83419A4 (3419A4;a-f), G248P86031A6 (6031A6;g-l), and G248P89065D8 (9065D8;m-r) as probes for the RNA (green) and BAC RP11-959I6 (a-r) as the probe for the DNA (red). In regions of the slides where the FISH worked well, the RNA FISH probes detected a positive signal in >90% of the cells for each probe. DNA was stained with DAPI. Arrows mark the location of RNA signal. Two sites of RNA hybridization (e and n) were detected in <5% of cells (see Fig. 4g).

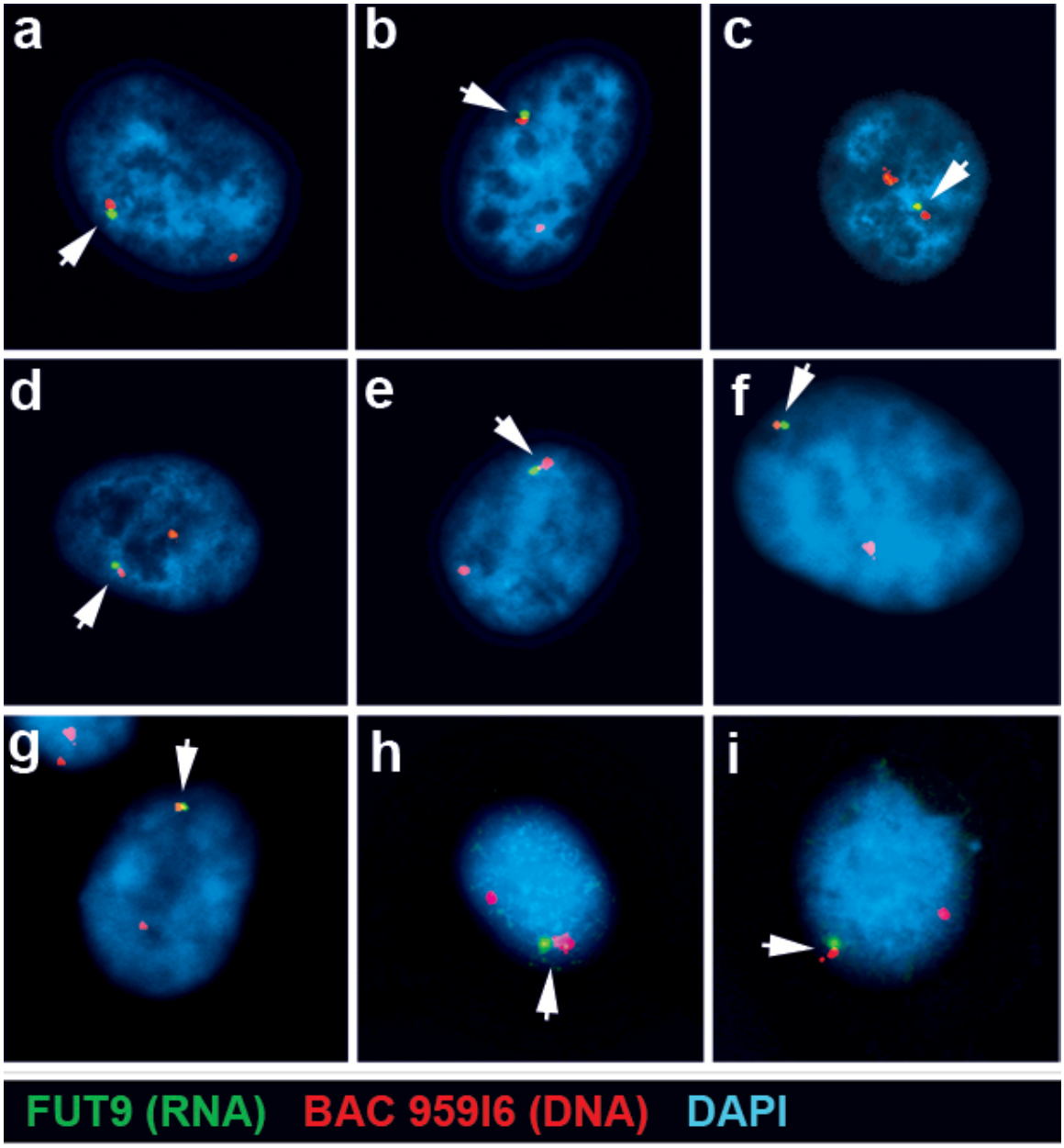

Sup. Fig. 28. RNA-DNA FISH for FUT9. P175 cells were subjected to RNA-DNA FISH using a FUT9 cDNA as probe for RNA (green) and BAC RP11-959I6 (a-r) as the probe for DNA (red). In regions of the slides where the FISH worked well, the RNA FISH probe detected a positive signal in >90% of the cells. DNA was stained with DAPI. Arrows mark the location of the RNA signal. Two sites of RNA hybridization were detected in <10% of cells (see Fig. 5f and 7d).

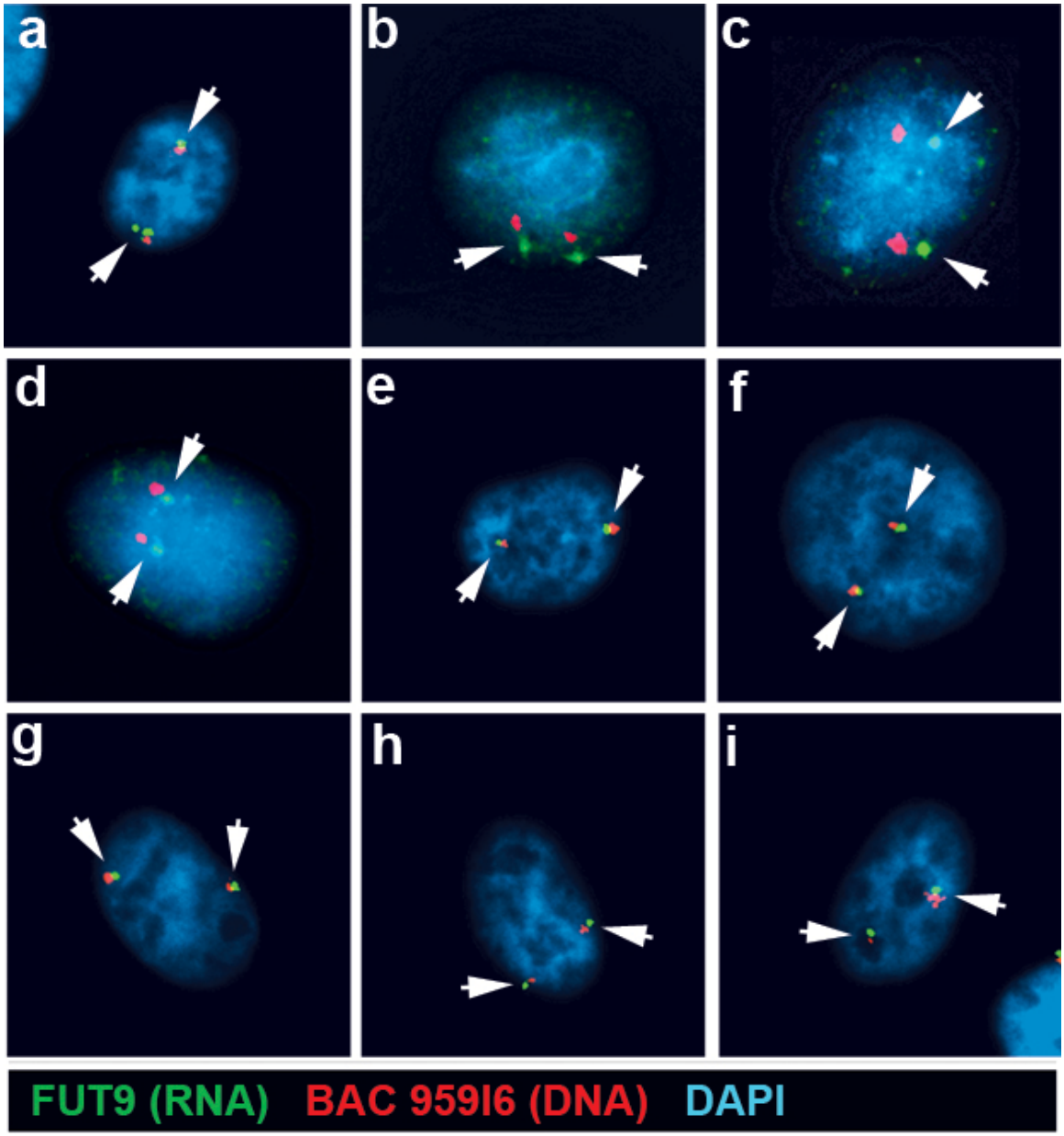

Sup. Fig. 29. RNA-DNA FISH for FUT9. Δ175-1i cells were subjected to RNA-DNA FISH using a FUT9 cDNA as probe for RNA (green) and BAC RP11-959I6 (a-r) as the probe for DNA (red). In regions of the slides where the FISH worked well, the RNA FISH probe detected a positive signal in >90% of the cells. DNA was stained with DAPI. Arrows mark the location of the RNA signal. Two sites of RNA hybridization were detected in >60% of cells (see Fig. 7c).

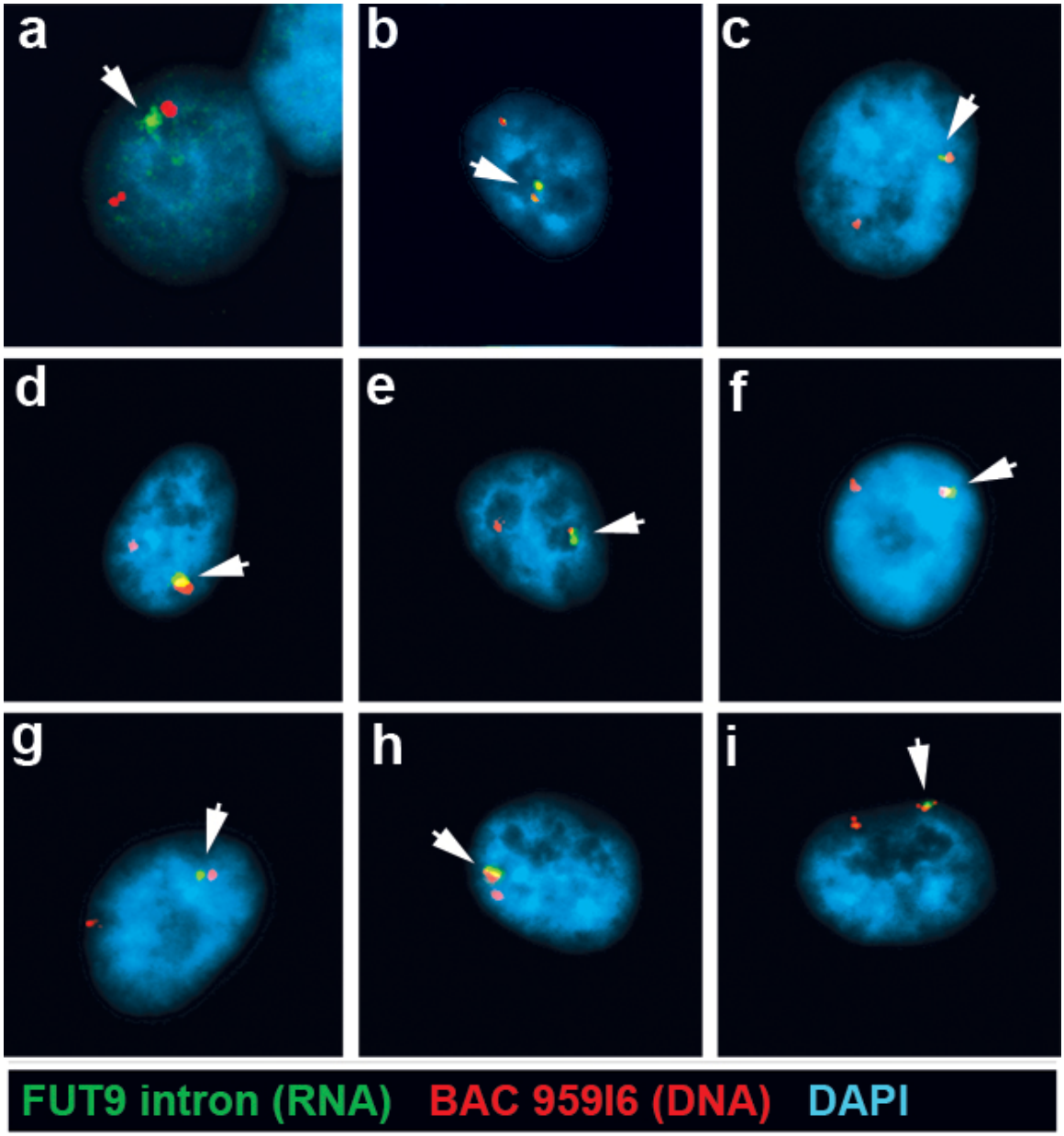

Sup. Fig. 30. RNA-DNA FISH for FUT9. P175 cells were subjected to RNA-DNA FISH using a 4.5 kb genomic fragment from the first intron of FUT9 as probe for RNA (green) and BAC RP11-959I6 (a-r) as the probe for DNA (red). In regions of the slides where the FISH worked well, the RNA FISH probe detected a positive signal in >90% of the cells. DNA was stained with DAPI. Arrows mark the location of the RNA signal. Two sites of RNA hybridization were detected in <10% of cells (see Fig. 4f and 7d).

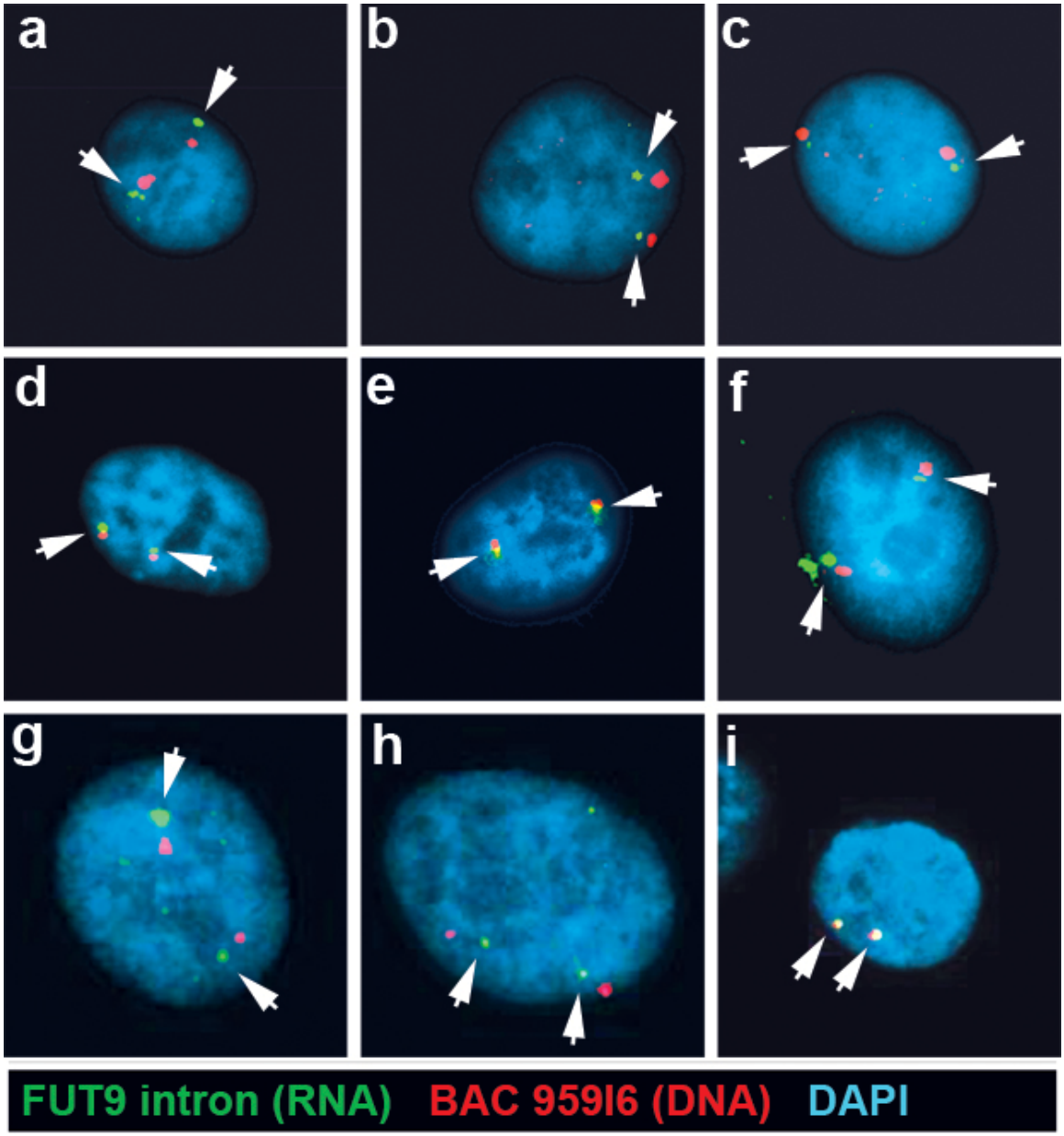

Sup. Fig. 31. RNA-DNA FISH for FUT9. Δ175-1i cells were subjected to RNA-DNA FISH using a 4.5 kb genomic fragment from the first intron of FUT9 as probe for RNA (green) and BAC RP11-959I6 (a-r) as the probe for DNA (red). In regions of the slides where the FISH worked well, the RNA FISH probe detected a positive signal in >90% of the cells. DNA was stained with DAPI. Arrows mark the location of the RNA signal. Two sites of RNA hybridization were detected in >55% of cells (see Fig. 7d).

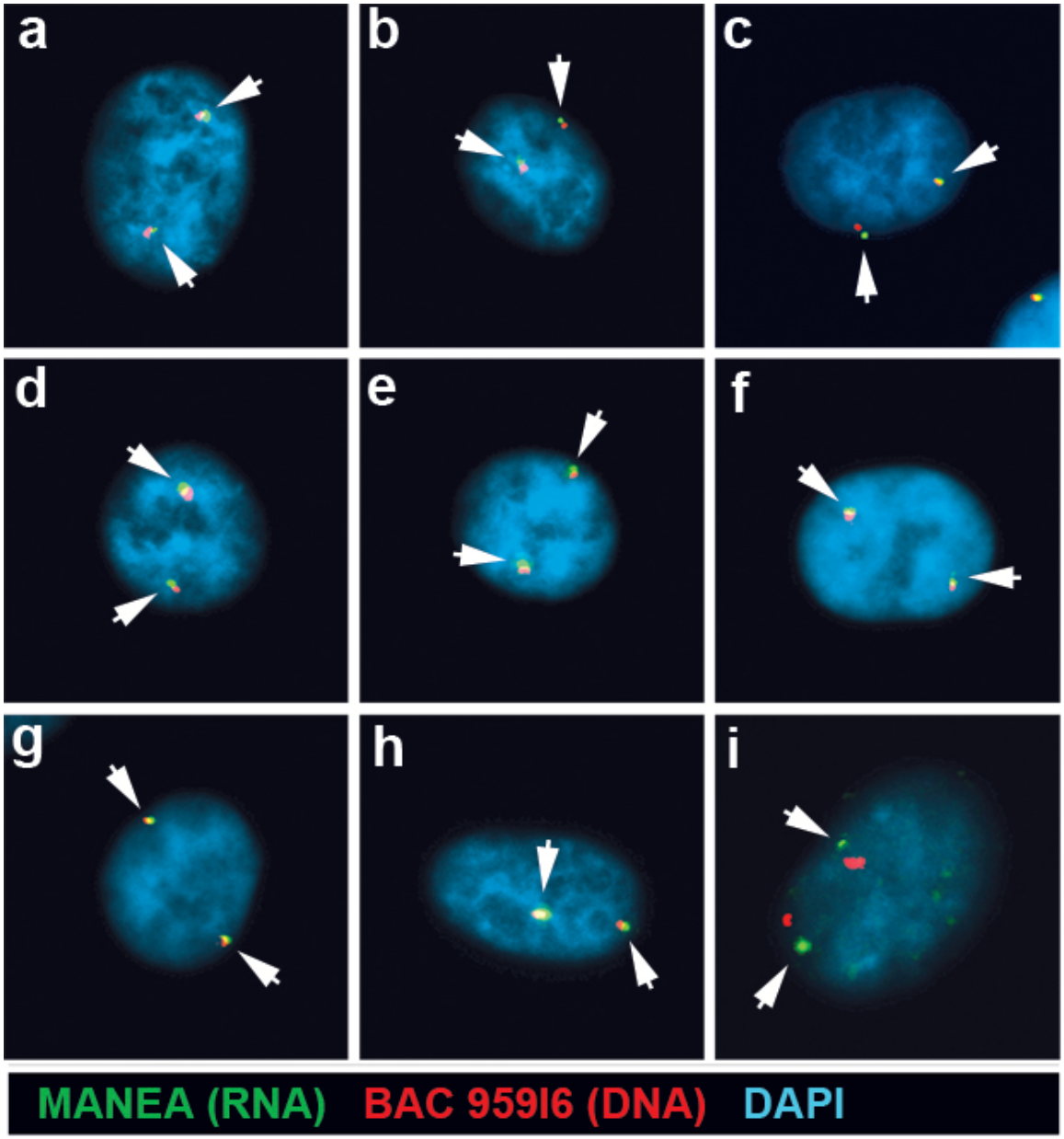

Sup. Fig. 32. RNA-DNA FISH for MANEA. P175 cells were subjected to RNA-DNA FISH using a MANEA cDNA as probe for RNA (green) and BAC RP11-959I6 (a-r) as the probe for DNA (red). In regions of the slides where the FISH worked well, the RNA FISH probe detected a positive signal in >90% of the cells. DNA was stained with DAPI. Arrows mark the location of the RNA signals. Two sites of RNA hybridization were detected in >70% of cells (see Fig. 5f).

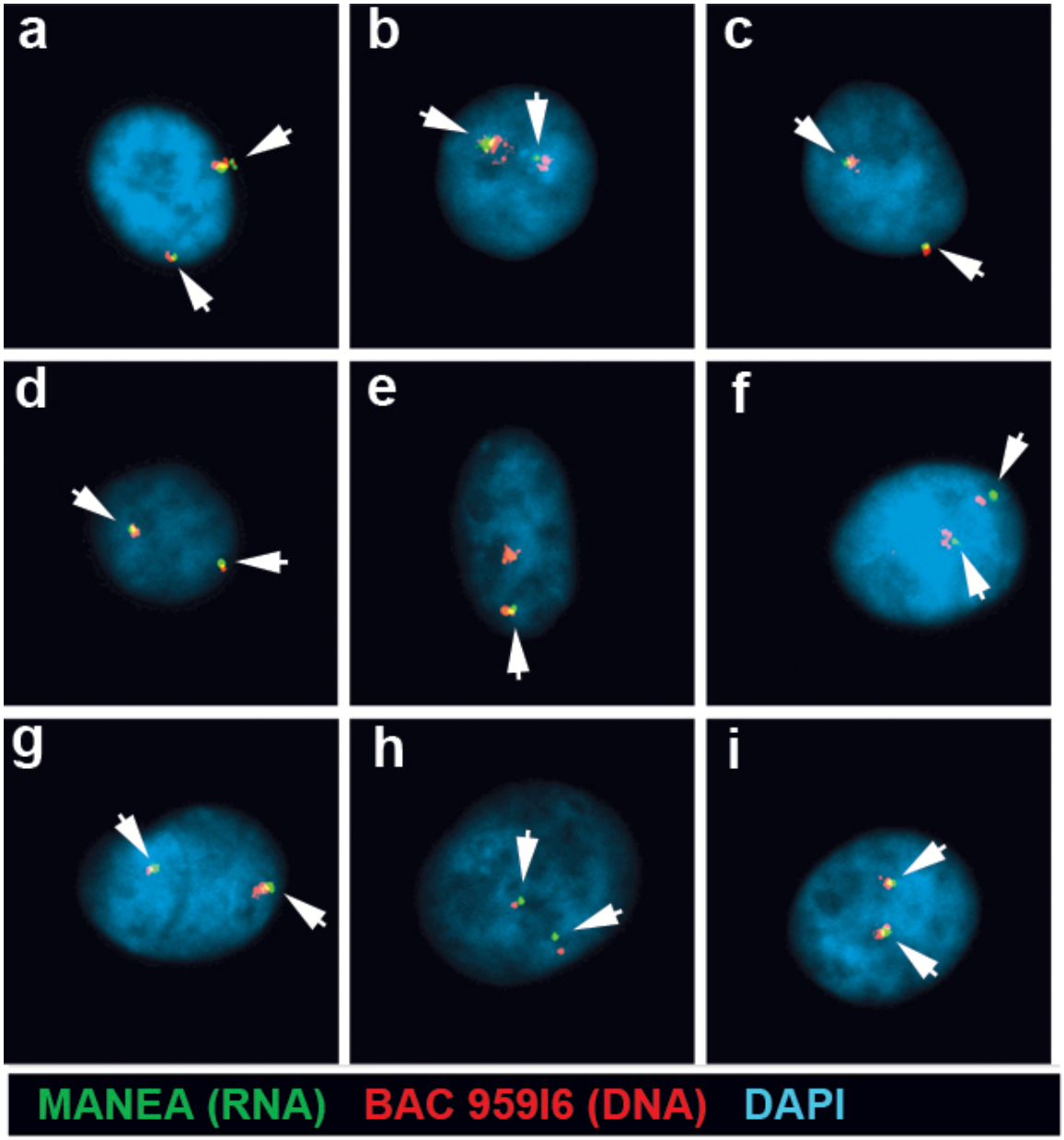

Sup. Fig. 33. RNA-DNA FISH for MANEA. Δ175-1i cells were subjected to RNA-DNA FISH using a MANEA cDNA as probe for RNA (green) and BAC RP11-959I6 (a-r) as the probe for DNA (red). In regions of the slides where the FISH worked well, the RNA FISH probe detected a positive signal in >90% of the cells. DNA was stained with DAPI. Arrows mark the location of the RNA signals. Two sites of RNA hybridization were detected in >75% of cells (see Fig. 7f).

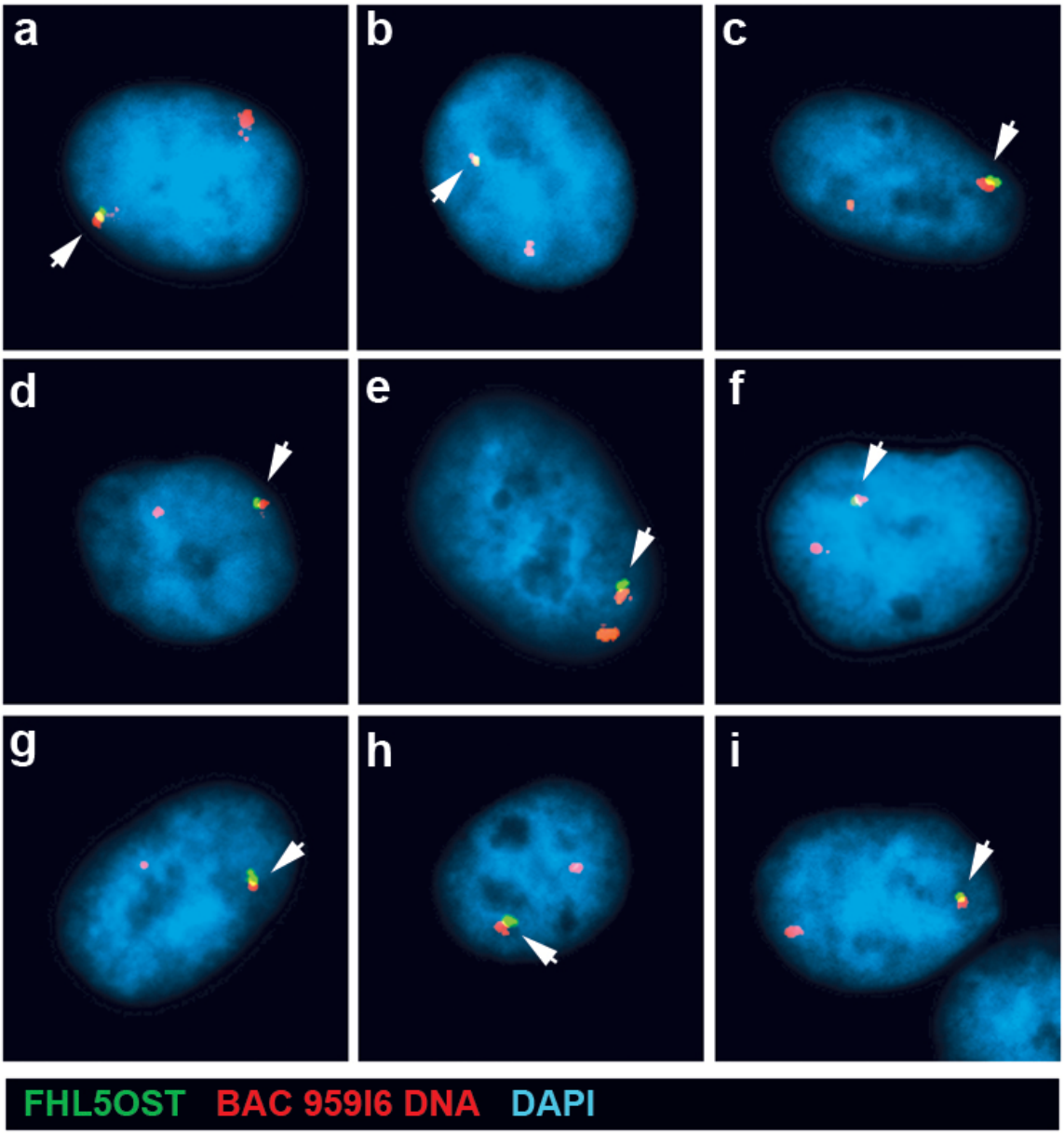

Sup. Fig. 34. RNA-DNA FISH for FHL5OST. P175 cells were subjected to RNA-DNA FISH using Fosmid G248P86054G4 as probe for RNA (green) and BAC RP11-959I6 (a-r) as the probe for DNA (red). In regions of the slides where the FISH worked well, the RNA FISH probe detected a positive signal in >90% of the cells. DNA was stained with DAPI. Arrows mark the location of the RNA signal. Two sites of RNA hybridization were detected in <15% of cells (see Fig. 7e).

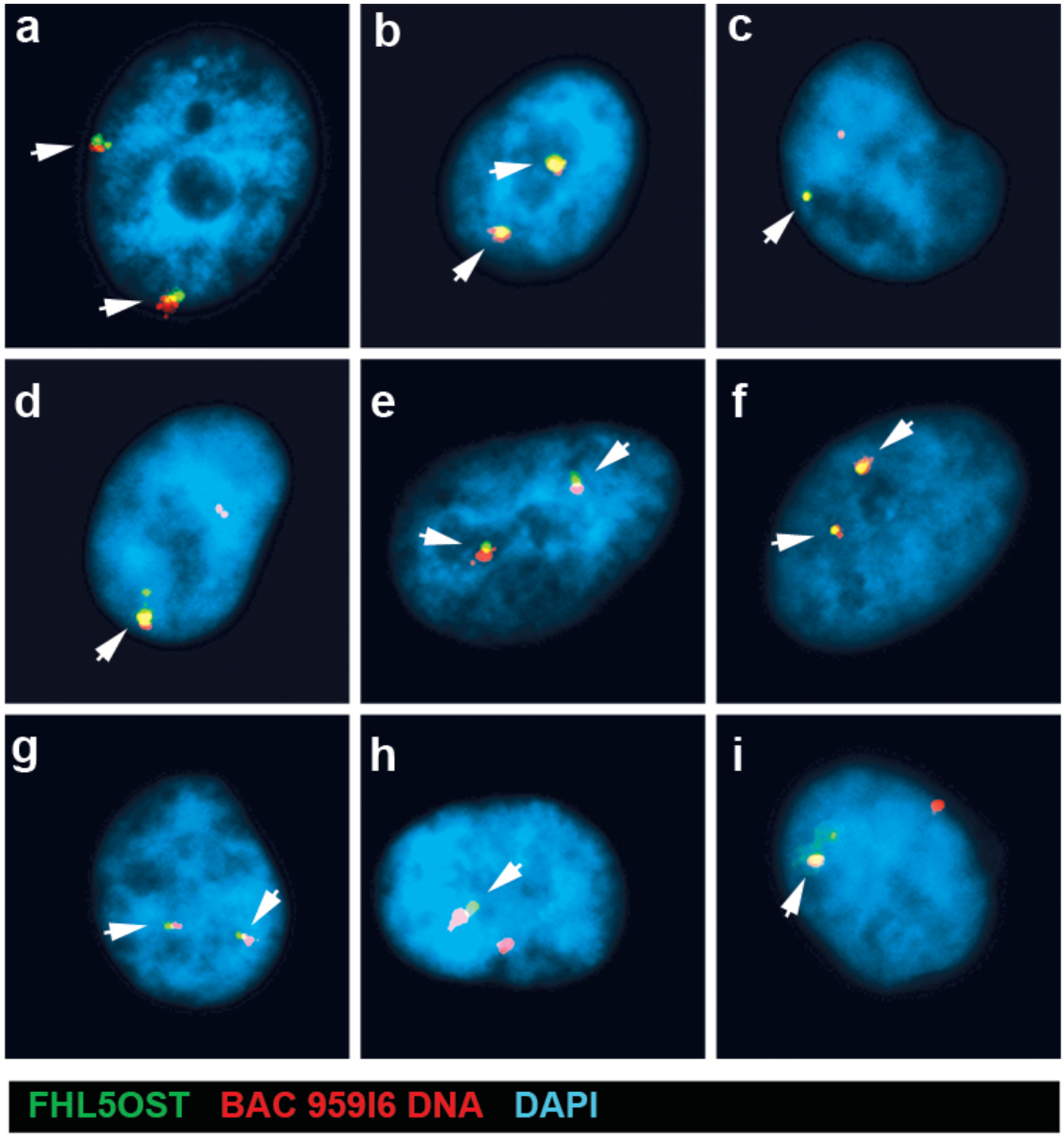

Sup. Fig. 35. RNA-DNA FISH for FHL5OST. Δ175-1i cells were subjected to RNA-DNA FISH using Fosmid G248P86054G4 as probe for RNA (green) and BAC RP11-959I6 (a-r) as the probe for DNA (red). In regions of the slides where the FISH worked well, the RNA FISH probe detected a positive signal in >90% of the cells. DNA was stained with DAPI. Arrows mark the location of the RNA signal. Two sites of RNA hybridization were detected in >50% of cells (see Fig. 7e).

Asynchronous replication timing on chromosome 6.

Chromosomal loci can be identified as replicating either synchronously or asynchronously using a FISH based assay [13]. FISH analysis of interphase nuclei pulse-labeled with BrdU allows selective examination of cells in S-phase. This assay also utilizes a methanol/acetic acid fixation, which destroys the nuclear structure and allows for an accurate estimate of replication timing [14, 15]. Using a probe to a particular chromosomal site, some cells display two single hybridization dots, indicating that neither allele has replicated (an SS pattern), other cells display two double dots, indicating that both alleles have replicated (a DD pattern), and a third class of cells contains one single dot and one double dot, indicating that only one of the two alleles (an SD pattern) has replicated. For this analysis, we used primary human skin fibroblasts and this FISH assay to quantify the number of hybridization signals per locus present in S-phase nuclei (Table 1). Supplemental Table 4 shows the BAC and Fosmid probes and the corresponding chromosomal positions for the loci used in this analysis. Supplementary Figure 35 shows examples of the SS, DD and SD patterns for ASAR6. In addition, using BAC probes for synchronously replicating loci [16], indicated that our assay scored the SD pattern within 2% of previously published data for both LARP (5q33.2) and C9orf43 (9q32) (see Table 1), indicating that our assay produced similar results as this previous study [16].

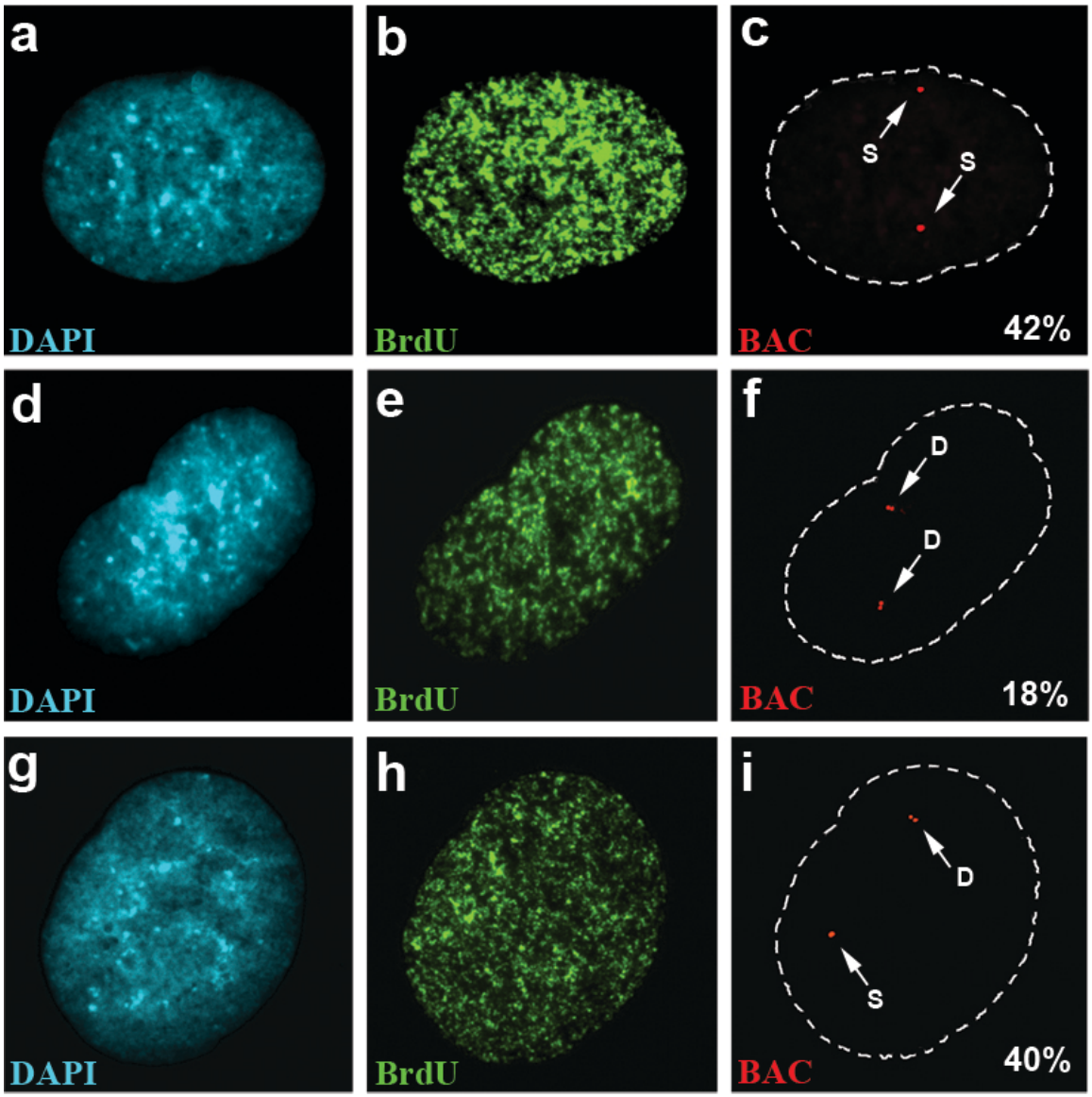

Sup. Fig. 36. DNA FISH replication assay. Low passage primary human skin fibroblast cells were pulse-labeled with BrdU for 60 minutes, harvested by trypsinization, fixed in 3:1 methanol:acetic acid, dropped on slides, and processed for DNA FISH using BAC RP11-374I15 as probe (red). BrdU was detected using an FITC labeled anti-BrdU antibody (green). DNA was stained with DAPI. Approximately 35% of cells were BrdU positive. Arrows mark the location of the DNA signals. Single dots (S) represent un-replicated loci and double dots (D) represent replicated loci. The frequency of the SS, DD and SD patterns were determined in 200 cells and are shown as percent (%).

Previous studies have also shown that the random mono-allelic genes present on autosomes are coordinated in their asynchronous replication so that

the alleles on one homolog replicate earlier than the alleles on the other [16, 17]. Therefore, we next tested if the asynchronously replicating loci present on chromosome 6 are also coordinated in their asynchronous replication. The level of coordination was examined using a two-color FISH assay and scoring cells that simultaneously displayed the SD pattern for both loci, essentially as described [16, 17]. The main text shows examples of coordination of asynchronous replication between ASAR6 and FUT9, FHL5, ME1, and HTR1E (see Fig. 6). Supplementary Figure 36 shows additional examples of coordination in asynchronous replication in cis between ASAR6 and the closely linked loci BAC959I6 (70/100 cells $P < 1 \times 10^{-4}$; Sup. Fig. 36a-c) and MANEA (78/100 cells $P < 1 \times 10^{-5}$; Sup. Fig. 36d-f), and an additional example of coordination in trans between ASAR6 and KCNQ5 (74/100 cells $P < 1 \times 10^{-5}$; Sup. Fig. 36g-i). In addition, Supplementary Figure 36 also shows examples of coordination in cis between the previously reported [18] mono-allelic genes ME1 and KCNQ5 (80/100 cells $P < 1 \times 10^{-5}$; Sup. Fig. 36j-l), and in trans between ME1 and FUT9 (80/100 cells $P < 1 \times 10^{-5}$; Sup. Fig. 36m-o). The fact that the assay did not show coordination in all cells suggests that, while the assay is robust ($P < 1 \times 10^{-4}$ for a deviation from 50% in the above examples), it does not allow visualization of the coordination in every cell examined.

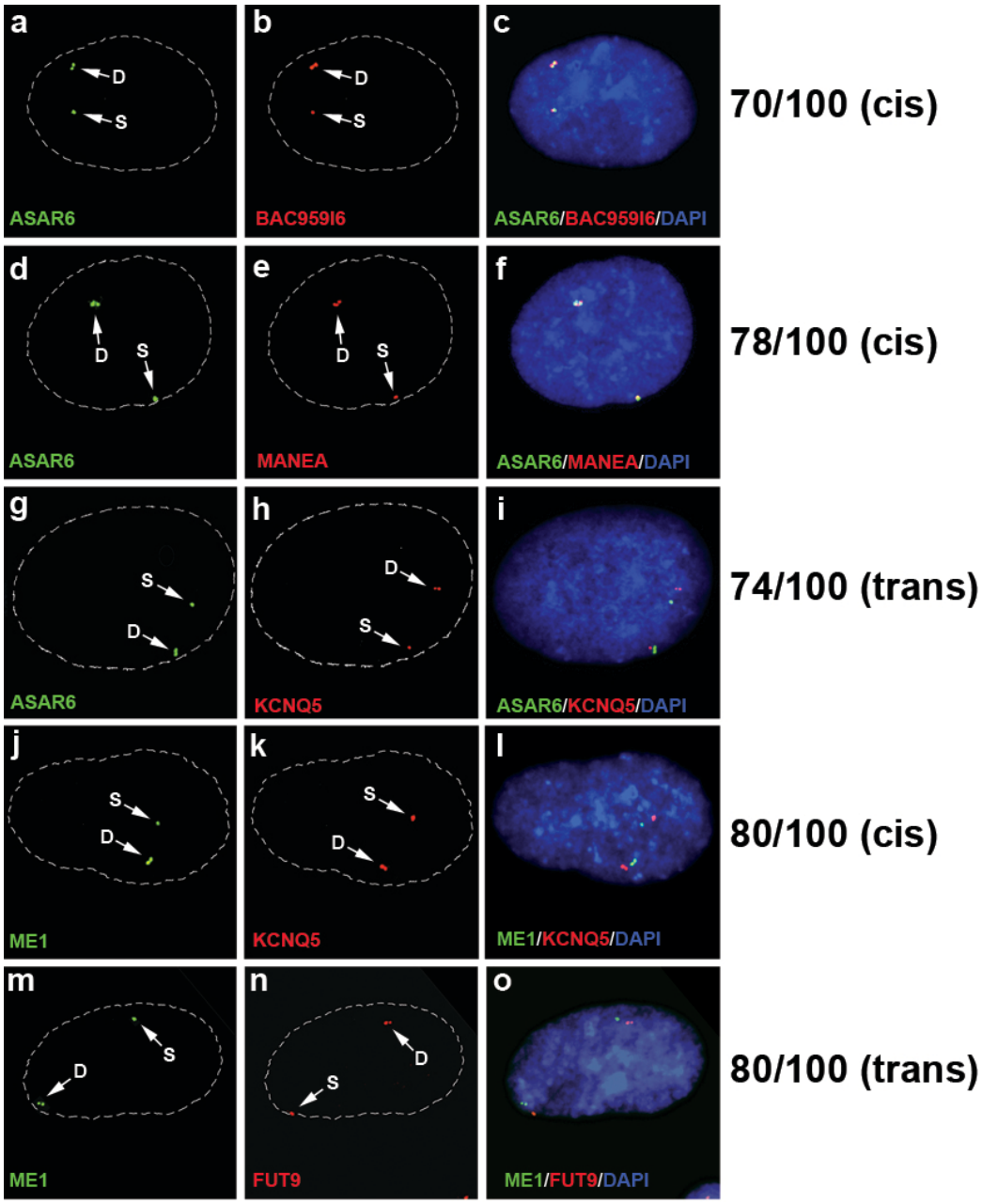

Sup. Fig. 37. Two-color DNA FISH assay for coordination in asynchronous replication. Low passage primary human skin fibroblasts were harvested by trypsinization, fixed in 3:1 methanol:acetic acid, dropped on slides, and processed for DNA FISH using BAC RP11-374I15 as probe (ASAR6; green; a-i) plus BAC959I6 (red; a-c), Fosmid G248P8476B7 (MANEA; red; d-f) or BAC RP11-106C24 (KCNQ5; red; g-i). FISH was also carried out with BAC RP11-703G14 as probe (ME1; green; j-o) plus BAC RP11-106C24 (KCNQ5; red; j-l) or BAC RP11-75N19 (FUT9; red; m-o). DNA was stained with DAPI. Arrows mark the location of the FISH signals. Single dots (S) represent un-replicated loci and double dots (D) represent replicated loci. 100 cells that simultaneously displayed the SD pattern for both probes were scored for the cis or trans configuration.

Our results indicate that ASAR6 is coordinated in its asynchronous replication timing in cis with the relatively closely linked loci MANEA, FUT9, BAC959I6, and FHL5/FHL5OST, suggesting that ASAR6 is located within a larger domain (>1 mb) of cis-coordinated replication timing. In addition, our data also show that ASAR6, and its larger replication-timing domain, is coordinated in asynchronous replication in trans with other chromosome 6 mono-allelic genes, located >8 mb either centromeric or telomeric to ASAR6. Thus the earlier replicating ASAR6 allele is coordinated with the later replicating alleles for HTR1E, KCNQ5, ME1, and FRK (see main text and Fig. 6).

Expression of MANEA, FHL5, FUT9, and ASAR6 in primary tissues.

To determine the tissue distribution of ASAR6 expression in relation to MANEA, FHL5, and FUT9 we used RT-PCR analysis on a panel of RNA samples isolated from various human tissues. Supplementary Figure 37 shows the RT-PCR analysis for expression of MANEA, FHL5, FUT9 and ASAR6 in the normal human tissue samples indicated. MANEA and FHL5 were expressed in all tissues assayed, while FUT9 and ASAR6 were expressed in a subset of tissues, including: brain, trachea, kidney, testes, and placenta. Interestingly, FUT9 shows a wider expression profile than ASAR6, also showing expression in bladder, prostate, and adipose tissues. This expression pattern for FUT9 is consistent with a previous report [19]. It will be interesting to determine if FUT9 is mono-

allelically expressed in the tissues that do not express ASAR6. Furthermore, it will be interesting to determine if disruption of the ASAR6 region also results in altered replication timing and bi-allelic expression of these and other mono-allelic genes on chromosome 6 in cells that do not express the ASAR6 transcripts.

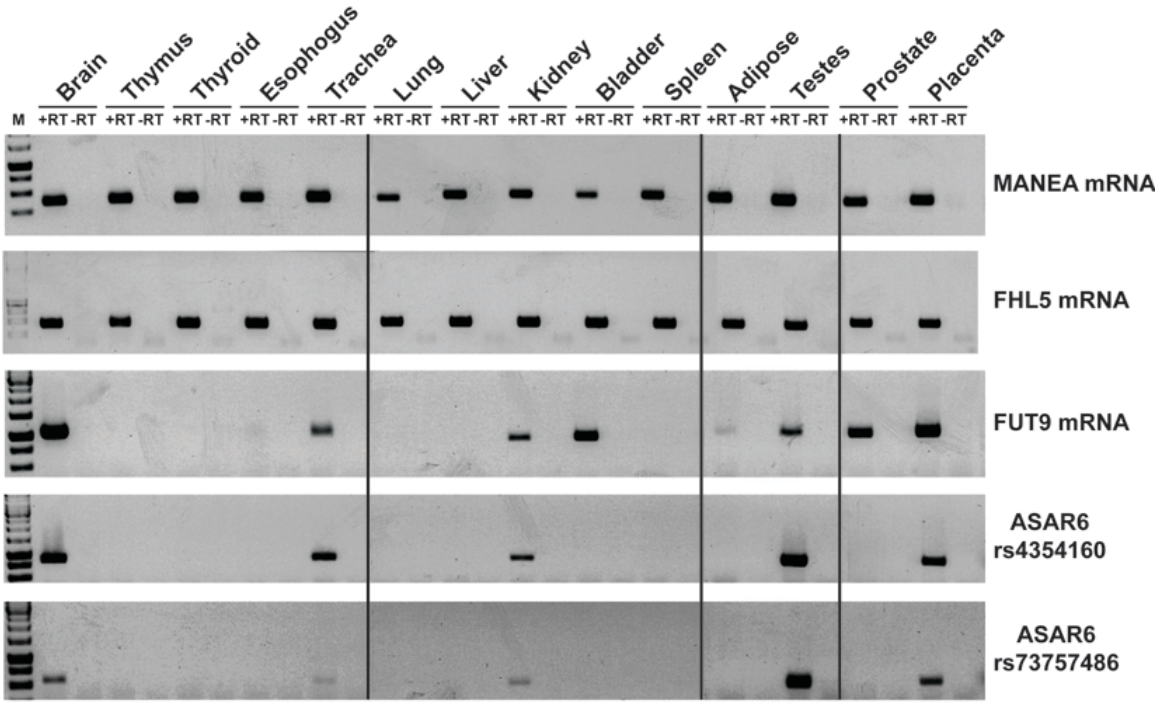

Sup. Fig. 38. Expression of MANEA, FHL5, FUT9 and ASAR6 in primary human tissues. Reverse transcriptase reactions, either with (+RT) or without (-RT) reverse transcriptase, on total RNA, were subjected to PCR with primers designed to span MANEA FHL5, and FUT9 exons and primers designed to amplify the rs2224951 and rs4354160 SNP locations within ASAR6 (see Sup. Tables 2 and 3). PCRs were carried out on first strand cDNA generated from total RNA isolated from the indicated tissues. Due to the large number of samples, multiple gels per primer set were run and the images inverted and combined using Photoshop. The black lines indicate the partition of individual gels.

Supporting References

1 Branda, C.S. and Dymecki, S.M. (2004) Talking about a revolution: The impact of site-specific recombinases on genetic analyses in mice. *Dev Cell*, **6**, 7-28.

2 Breger, K.S., Smith, L. and Thayer, M.J. (2005) Engineering translocations with delayed replication: evidence for cis control of chromosome replication timing. *Hum Mol Genet*, **14**, 2813-2827.

3 Breger, K.S., Smith, L., Turker, M.S. and Thayer, M.J. (2004) Ionizing radiation induces frequent translocations with delayed replication and condensation. *Cancer Research*, **64**, 8231-8238.

4 Zhu, Y., Bye, S., Stambrook, P.J. and Tischfield, J.A. (1994) Single-base deletion induced by benzo[a]pyrene diol epoxide at the adenine phosphoribosyltransferase locus in human fibrosarcoma cell lines. *Mutat Res*, **321**, 73-79.

5 Richardson, C. and Jasin, M. (2000) Frequent chromosomal translocations induced by DNA double-strand breaks. *Nature*, **405**, 697-700.

6 Mills, A.A. and Bradley, A. (2001) From mouse to man: generating megabase chromosome rearrangements. *Trends Genet*, **17**, 331-339.

7 Smith, L., Plug, A. and Thayer, M. (2001) Delayed Replication Timing Leads to Delayed Mitotic Chromosome Condensation and Chromosomal Instability of Chromosome Translocations. *Proc Natl Acad Sci U S A*, **98**, 13300-13305.

8 Chang, B.H., Smith, L., Huang, J. and Thayer, M. (2007) Chromosomes with delayed replication timing lead to checkpoint activation, delayed recruitment of Aurora B and chromosome instability. *Oncogene*, **26**, 1852-1861.

9 Camargo, M. and Cervenka, J. (1982) Patterns of DNA replication of human chromosomes. II. Replication map and replication model. *Am J Hum Genet*, **34**, 757-780.

10 Cohen, S.M., Cobb, E.R., Cordeiro-Stone, M. and Kaufman, D.G. (1998) Identification of chromosomal bands replicating early in the S phase of normal human fibroblasts. *Exp Cell Res*, **245**, 321-329.

11 Keim, M., Williams, R.S. and Harwood, A.J. (2004) An inverse PCR technique to rapidly isolate the flanking DNA of dictyostelium insertion mutants. *Mol Biotechnol*, **26**, 221-224.

12 Harkey, M.A., Kaul, R., Jacobs, M.A., Kurre, P., Bovee, D., Levy, R. and Blau, C.A. (2007) Multiarm high-throughput integration site detection: limitations of LAM-PCR technology and optimization for clonal analysis. *Stem Cells Dev*, **16**, 381-392.

13 Selig, S., Okumura, K., Ward, D.C. and Cedar, H. (1992) Delineation of DNA replication time zones by fluorescence in situ hybridization. *EMBO J*, **11**, 1217-1225.

14 Azuara, V., Brown, K.E., Williams, R.R., Webb, N., Dillon, N., Festenstein, R., Buckle, V., Merkenschlager, M. and Fisher, A.G. (2003) Heritable gene silencing in lymphocytes delays chromatid resolution without affecting the timing of DNA replication. *Nat Cell Biol*, **5**, 668-674.

15 Mostoslavsky, R., Singh, N., Tenzen, T., Goldmit, M., Gabay, C., Elizur, S., Qi, P., Reubinoff, B.E., Chess, A., Cedar, H. *et al.* (2001) Asynchronous replication and allelic exclusion in the immune system. *Nature*, **414**, 221-225.
16 Ensminger, A.W. and Chess, A. (2004) Coordinated replication timing of monoallelically expressed genes along human autosomes. *Hum Mol Genet*, **13**, 651-658.
17 Singh, N., Ebrahimi, F.A., Gimelbrant, A.A., Ensminger, A.W., Tackett, M.R., Qi, P., Gribnau, J. and Chess, A. (2003) Coordination of the random asynchronous replication of autosomal loci. *Nat Genet*, **33**, 339-341.
18 Gimelbrant, A., Hutchinson, J.N., Thompson, B.R. and Chess, A. (2007) Widespread monoallelic expression on human autosomes. *Science*, **318**, 1136-1140.
19 Cailleau-Thomas, A., Coullin, P., Candelier, J.J., Balanzino, L., Mennesson, B., Oriol, R. and Mollicone, R. (2000) FUT4 and FUT9 genes are expressed early in human embryogenesis. *Glycobiology*, **10**, 789-802.